Meteorol. Z. (Contrib. Atm. Sci.), Vol. **30**, No. 1, 9–32 (published online December 9, 2019)

DACH 2019

Thermal conditions during heat waves of a mid-European metropolis under consideration of climate change, urban development scenarios and resilience measures for the mid-21st century

Heidelinde Trimmel[1,6*], Philipp Weihs[1], Stéphanie Faroux[2], Herbert Formayer[1], Paul Hamer[6], Kristofer Hasel[1,4], Johannes Laimighofer[5], David Leidinger[1], Valéry Masson[2], Imran Nadeem[1], Sandro M. Oswald[1,3], Michael Revesz[1] and Robert Schoetter[2]

[1]Institute of Meteorology and Climatology, University of Natural Resources and Life Sciences (BOKU), Vienna, Austria
[2]CNRM, Université de Toulouse, Météo-France, Toulouse, France
[3]Zentralanstalt für Meteorologie und Geodynamik (ZAMG), Vienna, Austria
[4]Department of Meteorology and Geophysics, University of Vienna, Vienna, Austria
[5]Institute of Statistics, University of Natural Resources and Life Sciences (BOKU), Vienna, Austria
[6]Norsk institutt for luftforskning (NILU), Kjeller, Norway

(Manuscript received June 9, 2019; in revised form October 25, 2019; accepted October 28, 2019)

Abstract

In this study we produce two urban development scenarios estimating potential urban sprawl and optimized development concerning building construction, and we simulate their influence on air temperature, surface temperatures and human thermal comfort. We select two heat waves representative for present and future conditions of the mid 21st century and simulations are run with the Town Energy Balance Model (TEB) coupled online and offline to the Weather Research and Forecasting Model (WRF). Global and regional climate change under the RCP8.5 scenario causes an increase of daily maximum air temperature in Vienna by 7 K. The daily minimum air temperature will increase by 2–4 K. Changes caused by urban growth or densification mainly affect air temperature and human thermal comfort locally where new urbanisation takes place and does not occur significantly in the central districts. A combination of near zero-energy standards and increasing albedo of building materials on the city scale accomplishes a maximum reduction of urban canyon temperature achieved by changes in urban parameters of 0.9 K for the minima and 0.2 K for the maxima. Local scale changes of different adaptation measures show that insulation of buildings alone increases the maximum wall surface temperatures by more than 10 K or the maximum mean radiant temperature (MRT) in the canyon by 5 K. Therefore, measures to reduce MRT within the urban canyons like tree shade are needed to complement the proposed measures. This study concludes that the rising air temperatures expected by climate change puts an unprecedented heat burden on Viennese inhabitants, which cannot easily be reduced by measures concerning buildings within the city itself. Additionally, measures such as planting trees to provide shade, regional water sensitive planning and global reduction of greenhouse gas emissions in order to reduce temperature extremes are required.

Keywords: urban sprawl, climate change, heat waves, urban scenarios, resilience, TEB, WRF, UTCI

1 Introduction

The urban environment influences the atmospheric conditions at the surface in various ways. Air temperature is higher mainly at night in comparison to rural areas, which is well known as the urban heat island effect, (UHI, Landsberg, 1981; Oke, 1982; Grimmond et al., 2010). In addition, vapour pressure or specific humidity can be lower due to reduced water availability, and the radiation and wind fields are strongly altered by the three-dimensional building structures (Grimmond et al., 2010).

These effects might further increase due to strong urbanization trends, which includes densification and growth of existing urban agglomerations. For instance, until 2030, the population within the metropolitan area of Vienna is expected to increase by 10 % (ÖROK, 2017). This will cause an increase in the demand for gross floor area resulting in urban densification and/or urban expansion. However, even under current conditions, the population in Vienna is suffering from heat

*Corresponding author: Heidelinde Trimmel, Institute of Meteorology and Climatology, University of Natural Resources and Life Sciences (BOKU), Gregor Mendelstrasse 33, 1180 Vienna, Austria, e-mail: heidelinde.trimmel@boku.ac.at

DOI 10.1127/metz/2019/0966
Gebrüder Borntraeger Science Publishers, Stuttgart, www.borntraeger-cramer.com

stress during the summer months (Matzarakis et al., 2011; Muthers et al., 2010; MA 22, 2018). In the present article, we research the impact of the projected urban development in Vienna on human thermal comfort.

Rises in air temperature that can be expected due to climate change (APCC, 2014) present an additional threat to human thermal comfort in the urban realm. Air temperature has been rising and is expected to continue to rise globally within the next century (IPCC, 2013). In eastern Austria, mean air temperature has risen by 2 K since 1880, which is more than double the 0.85 K rise recorded globally (Auer et al., 2014). Emission scenario A1B projects that by the end of the 21st century mean air temperature increases of 3.5 K above the level of the reference period 1961–1990 are expected in Austria (APCC, 2014; Gobiet et al., 2014). Cities themselves contribute to climate change by the emissions caused by e.g., ground and air traffic, industrial processes, heating, electricity generation, waste and production of building material (De Pee et al., 2018; Bardow and Green, 2018; Kennedy et al., 2009).

Heat waves have been recognized as a lethal threat to humans around the world within the last decades (McMichael et al., 2003; Valleron and Boumendil, 2004; Kim and Kyselý, 2009; Grimmond et al., 2010: Gabriel and Endlicher, 2011) and also Vienna (Hutter et al., 2007). Additionally, the combination of the elevated air temperature during heat waves and high irradiation (Otani et al., 2017; Schreier et al., 2013), humidity (Steadman, 1979a, b) or air pollution (Kalisa et al., 2018; Schnell and Prather, 2017; Zhang et al., 2017) poses a threat to human health.

It has been found that the heat wave length and intensity will increase in the future, e.g., for Paris (Lemonsu et al., 2013) and also for Vienna (Formayer et al., 2007). Kyselý days are defined as days of a heatwave period, which is characterised by at least three subsequent days with daily maximum air temperature larger than 30 °C and continues until the daily maximum air temperature drops below 25 °C or until the mean daily maximum air temperature of the period drops below 30 °C (Kyselý et al., 2000). An increase of the number of Kyselý days by up to a factor of 10 from 1961–1990 to the end of the 21st century is expected by Formayer et al. (2007) for Vienna (Scenario A2, Model: HadRM3H; Jones et al., 2001). This alarming fact has caused various heat warning systems to be developed (Michelozzi et al., 2004; Tan et al., 2007).

To be able to project the thermal strain caused by future heat waves and urban growth it is necessary to have the appropriate tools that can take into account as many of the involved physical processes as possible (especially in the context of a changing climate). This includes microscale processes such as reflections within the urban canyon, wind reduction, energy uptake and storage in roads and buildings resolved, e.g., by the town and energy balance scheme TEB (Masson, 2000; Masson et al., 2002; Bueno et al., 2012; Pigeon et al., 2014). Furthermore, representations of evapotranspiration by urban vegetation, which have been implemented in TEB (Lemonsu et al., 2012; DeMunck et al., 2013), city scale effects caused by spatial inhomogeneity (e.g., potential thermal breezes), and topography (e.g., topographically-generated or modified winds) are of key importance. Finally, the interaction between the surface layer and the atmosphere and its effects on the evolution of the urban boundary layer are crucial (Oke, 1987; Stull, 1988, Bornstein and Lin, 2000; Grimmond et al., 2010) as it is done in atmospheric models, e.g., the weather research and forecasting model WRF (Skamarock et al., 2008).

In this study we will work with resilience measures, because we want to point out that the aim of urban development should be to make the city more resilient – or to better cope and maintain function during climatic extremes (Zommers and Alverson, 2018). Resilience covers the more holistic approach of urban planning (Sharifi and Yamagata, 2018; Ürge-Vorsatz et al., 2018). Here, we will apply some basic changes in material properties as a first and important step to help to reduce thermal strain in urban agglomerations and thus increase resilience.

To measure the subjective perception of temperature there are many indices describing human thermal comfort (PMV (Fanger, 1970), PET (Mayer and Höppe, 1987), UTCI (Fiala et al., 2001; Bröde et al., 2012; Jendritzky et al., 2012)), heat stress or apparent temperature (humidex, wind chill, wet-bulb globe temperature). Generally important factors for the human organism are the radiation received by humans, the ambient air temperature, humidity and wind speed (Mayer and Höppe, 1987). There is a positive relationship between human thermal stress and increasing MRT for the warm part of the thermal comfort spectrum. In this thermal comfort range the relation to air temperature and water vapour pressure even increases with higher air temperatures (Dou, 2014). In this study the Universal Thermal Climate Index (UTCI) is used.

The aim of this article is, to present:

1. The setup of a mesoscale meteorological model coupled to an urban energy balance model (Section 2.1)

2. Future urban scenarios for Vienna (Section 2.3 and 2.4)

3. The change of the 2 m air temperature for a selected present and a future heat wave on city level (Section 3.1):

   - Daily maximum temperature, as a factor for human thermal strain
   - Daily minimum temperature, to quantify the nocturnal canopy urban heat island (CUHI) magnitude
   - The influence of urban sprawl and densification

4. Analysis of the effects of different resilience measures on a local level (Section 3.2):
   - Energy flux differences, which are transferred from the urban surface to the atmospheric model
   - The surface temperatures of roof, wall and road, to understand the air temperature changes
5. Analysis of canyon parameters to estimate thermal strain in the idealized canyon (Section 3.3)

We do not address the detail planning within the street canyons, but urban development regarding urban material choice, distribution and density of built land on a scale > 100 m.

2 Materials and methods

2.1 Modelling Framework

In this study, the open-source mesoscale atmospheric model WRFv3.9.1 (Skamarock et al., 2008) is used in combination with an urban canopy model called the Town Energy Balance (TEB; Masson, 2000; Masson et al., 2002) model. Both models are coupled and run online. Additionally, offline simulation runs were done by forcing TEB as it is integrated in SURFEXv8 (Boone et al., 2017) with the output of WRF-TEB.

WRF is used to downscale the ECMWF Analysis Data Set for present-day conditions (temporal resolution of 6 hours, horizontal resolution of 9 km (https://www.ecmwf.int/en/forecasts/datasets/set-i) via two intermediate nests (3 km and 1 km resolution) using one-way grid nesting to a 333 m resolution domain covering the city of Vienna (Figure A-1). There are 40 vertical levels in the WRF simulations, thereof 7 below 1000 m. For the topographical elevation, the SRTM1Arc:30 m data set is used. The Yonsei University Scheme is used for the Planetary Boundary Layer scheme together with the NOAH Land Surface Model to model the land-atmosphere interaction. For the land cover information, the Corine data (EEA, 2012) was reclassified to USGS classes (30 non-urban, 3 urban) (Table B-1) in order to be consistent with WRF (Schicker et al., 2016).

For the future heat wave conditions, we use selected events from regional climate model simulations forced by different representative concentration pathways (RCPs) to force our WRF-TEB simulations. The details of the regional climate model simulations, the heat wave selection process, and the coupling with WRF are described in Section 2.5.

Our different future urban development scenarios representing urban densification and sprawl are created by modifying the Corine land surface dataset using specific information regarding expected urban growth. The details of these urban development scenarios, and how they are created and applied is described in Section 2.4.

TEB version 1.1550 is implemented in the Weather Research and Forecasting (WRF) model. The Town Energy Balance (TEB) model developed by Masson (2000) is a physically based single-layer urban canopy scheme that is designed for urban surface parameterization of atmospheric models. The building energy model (BEM) that has been integrated in the TEB scheme (Bueno et al., 2012) is also deployed in the coupling. BEM-TEB makes it possible to represent the energy effects of buildings and building systems on the local urban climate and to provide estimations of the building energy consumption at the city scale with a resolution of down to 100 m.

The TEB scheme takes meteorological parameters at the lowest level of WRF as input. These parameters are air temperature and specific humidity, wind speed and direction, air pressure, direct and diffuse downwelling solar radiation, downwelling longwave radiation and precipitation. In return, TEB provides roof, road and wall temperature, emissivity, latent, sensible heat and momentum fluxes to the WRF model as output. In addition, 2-m temperature, 2-m humidity, and 10-m wind are obtained from the diagnosed TEB canyon temperature, humidity, and wind, respectively.

The URBPARAM.TBL and registry files in WRF have also been modified to accommodate urban parameters required by TEB-BEM and to write out urban parameters in the model output. All necessary conversions (e.g., specific humidity to mixing ratio) are done. We use the canyon temperature calculated by TEB for the calculation of the 2 m air temperature of WRF-TEB within urban areas. The coupled model WRF-TEB uses the same spatial resolution as the original WRF.

Offline simulations using SURFEXv8 were done due to different reasons. First, the simulation time was much faster and so more resilience measures could be simulated, as would have been possible with the online version, second some resilience measures (green roofs and photovoltaic on roofs) have not been implemented in WRF-TEB, but in SURFEXv8 and third SURFEXv8 offers the calculation of the thermal index UTCI. We analysed various results from the offline simulations: the energy fluxes, surface temperature, canyon air temperature, mean radiant temperature and UTCI. Here, mainly shaded UTCI is used, which is the UTCI calculated only from influences by diffuse radiation, without the direct component. Therefore, it can also be calculated when no buildings are present. The direct component is so pronounced, that in this study we found that there is no way to improve the UTCI in the sun during summer heat waves, only conditions can be made more bearable in the shadow.

2.2 Validation and uncertainties

The energy fluxes and surface temperatures of roof, wall and road temperatures calculated by TEB have been validated by Masson et al. (2002) for Vancouver and Mexico City. For Mexico City the road and roof temperatures showed a bias of 4 and 1.9 K, and a RMSE of 4.2 and 4.5 K. The radiation, turbulent (sensible+latent) and

storage fluxes showed a bias of 10, −3 and 13 W m^{-1}, respectively, and a RMSE of 32, 25 and 38 W m^{-1}. For Vancouver the wall and roof temperatures showed a bias of 2.3 and 2.5 K and a RMSE of 3 and 7.3 K. Further TEB was validated for Marseille (Lemonsu et al., 2004), Ouagadougou (Offerle et al., 2005) and cold climates, which is not relevant here. The BEM was validated by Pigeon et al. (2014) for Paris. In addition, we validated the 2 m air temperature in different Viennese urban canyons and found a mean absolute error for WRF-TEB between 0.99 and 1.51 K, and the RMSE was between 1.3 and 1.89 (Table A-1).

The water vapour pressure calculated from WRF-TEB is compared to measurements at Wien Hohe Warte (Figure A-7) and Wien Innere Stadt (Figure A-8). An RMSE of 2.68 and 2.03, a bias of 1.55 and 0.28, respectively, were found. Under the circumstances described above, the imprecisions lead to an uncertainty of 0.2–0.3 K in the UTCI.

If we use the meteorological conditions of the future heat wave to estimate the forward propagation of a potential error of air temperature in the range of the calculated RMSE of 1.9 K, then we find that the UTCI increases directly with the air temperature, so this error would result in an increase of 1.9 K in UTCI as well.

The MRT and UTCI calculated by TEB was compared with the results of the higher spatially resolved model SOLWEIG. The validation is described in more detail in Annex A.

2.3 Definition of urban parameters of Vienna

In order to run the simulations, the urban parameters were derived for Vienna. First, they were obtained for the finest available scale, then aggregated on block scale of the Viennese municipal land use map (Realnutzungskartierung – https://www.wien.gv.at/stadtentwicklung/grundlagen/stadtforschung/siedlungsentwicklung/realnutzungskartierung/pdf/rnk-2012.pdf). This method was oriented on the study by Cordeau (2016) and a graphical overview can also be found in the Annex (Figure B-1). The surface ratios of built, sealed and unsealed surface were derived from the highly detailed vector land cover data set (Flächenmehrzweckkarte – Viennese building height model (Baukörpermodell – https://www.wien.gv.at/stadtentwicklung/stadtvermessung/geodaten/bkm). Building roughness height was estimated as 1/10th of building height. The vertical to horizontal wall ratio was calculated using the above-mentioned vector data sets. The physical building parameters were derived by linking a dataset of building age and typology with typical building parameters obtained from different studies (Berger et al., 2012; Amtmann and Altmann-Mavaddat, 2014) and the OIB (Austrian Institute of Construction Engineering). More information about the mapping of physical building parameters can be found in Annex B. Because the selected outer model domain covers 417 km × 297 km (Figure A-1) and thus is much larger than the area for which the LCZ map could be produced and WRF is not able to include all LCZ classes, so the Corine 2012 data set was used in this study. Unlike the LCZs and the UrbanAtlas, Corine 2012 is available for all WRF domains, and there is existing methodology for how to use Corine in WRF (Pineda et al., 2004; Schicker et al., 2016). Corine is updated every 6 years. After this there might be even update cycles of 5 years, which makes it a very useful dataset.

While the standard version of WRF reclassifies Corine to USGS classes and thereby regroups all urban classes of Corine (1–11) to one urban class (Pineda et al., 2004), WRF-TEB is enhanced to support the use of 3 urban classes. In order to take into account non-built and vegetated urban areas, some urban classes of Corine are reclassified to USGS Nature classes (Table B-1). The parameters are thus extracted for these classes. The final model setup is listed in Table B-2.

2.4 Urban Scenarios

In this study next to the actual Corine land use data set two adapted "future" Corine data sets were created which show differing urban distributions (see Annex C). A further additional five scenarios, where only urban parameters were changed are prepared (2.4.2). An overview of the parameters used is given in Table 1. The "reference scenario" (REF) is the base scenario and shows the distribution of urban area according to the Corine 2012 data set, generalized to USGS Classes (Fig. 1a). The two urban development scenarios "urban sprawl" (SPR) and "optimized city" (OPT) both assume the same increase of population and estimated gross floor area demand (see Annex C, Table C-1), but under different spatial distribution (see Annex C, Table C-2). SPR assumes the same material property as REF. OPT uses modified urban parameters as described in Section 2.4.1.

2.4.1 Change in material properties

Apart from the spatial changes, the OPT scenario differs in two aspects, which are intended to represent selected effective resilience measures which can potentially be implemented in Vienna to counteract climate change and to reduce the urban heat island within the possibility of the modelling framework (Table 1). This reduction is aimed to be achieved mainly by reduction of heat uptake by increasing reflection and by preventing heat transfer into the building and not by increasing the latent heat flux to avoid sultriness, which can play an important role at high air temperatures (Steadman, 1979a, b). Tree shade, which is a very important measure to improve human thermal comfort at street level could not be included in the study due to model constraints. It is assumed that the same resilience measures are applied to all three urban categories to obtain maximum effects.

Table 1: Overview of all presented scenarios: reference scenario (REF), the urban development scenarios: urban sprawl (SPR), optimized city (OPT), the resilience measure scenarios: increased albedo (ALB), decreased thermal conductivity of urban materials (INS), increased urban density (DEN), implementation of green roofs (GRR), installation of photovoltaic panels on roofs (PVR).

Name of urban scenario:	REF	SPR	OPT	ALB	INS	DEN	GRR	PVR
Total built urban area [km^2]	929	1115	939	929	929	929	929	929
relative to "REF" [%]	100 %	120 %	101 %	100 %	100 %	100 %	100 %	100 %
built area in urban category:								
low density residential [%]	22	22	24.2	22	22	24.2	22	22
high density residential [%]	46	46	46.2	46	46	46	46	46
commercial [%]	16	16	24.2	16	16	24.2	16	16
Thermal conductivity, roof [W/mK]	1.7	1.7	0.1	1.7	0.1	1.7	1.7	1.7
Thermal conductivity, wall [W/mK]	1.4	1.4	0.1	1.4	0.1	1.4	1.4	1.4
Thermal conductivity, ground [W/mK]	0.9	0.9	0.4	0.9	0.4	0.9	0.9	0.9
Albedo, roof [–]	0.15	0.15	0.68	0.68	0.15	0.15	0.154	0.1
Albedo, wall [–]	0.2	0.2	0.3	0.3	0.2	0.2	0.2	0.2
Albedo, ground [–]	0.138	0.138	0.3	0.3	0.138	0.138	0.138	0.138
Green roof fraction [–]	0	0	0	0	0	0	1	0
Photovoltaic fraction on roofs [–]	0	0	0	0	0	0	0	1
WRF-TEB online forcing for SURFEX offline simulations	REF	SPR	OPT	REF	REF	REF	REF	REF

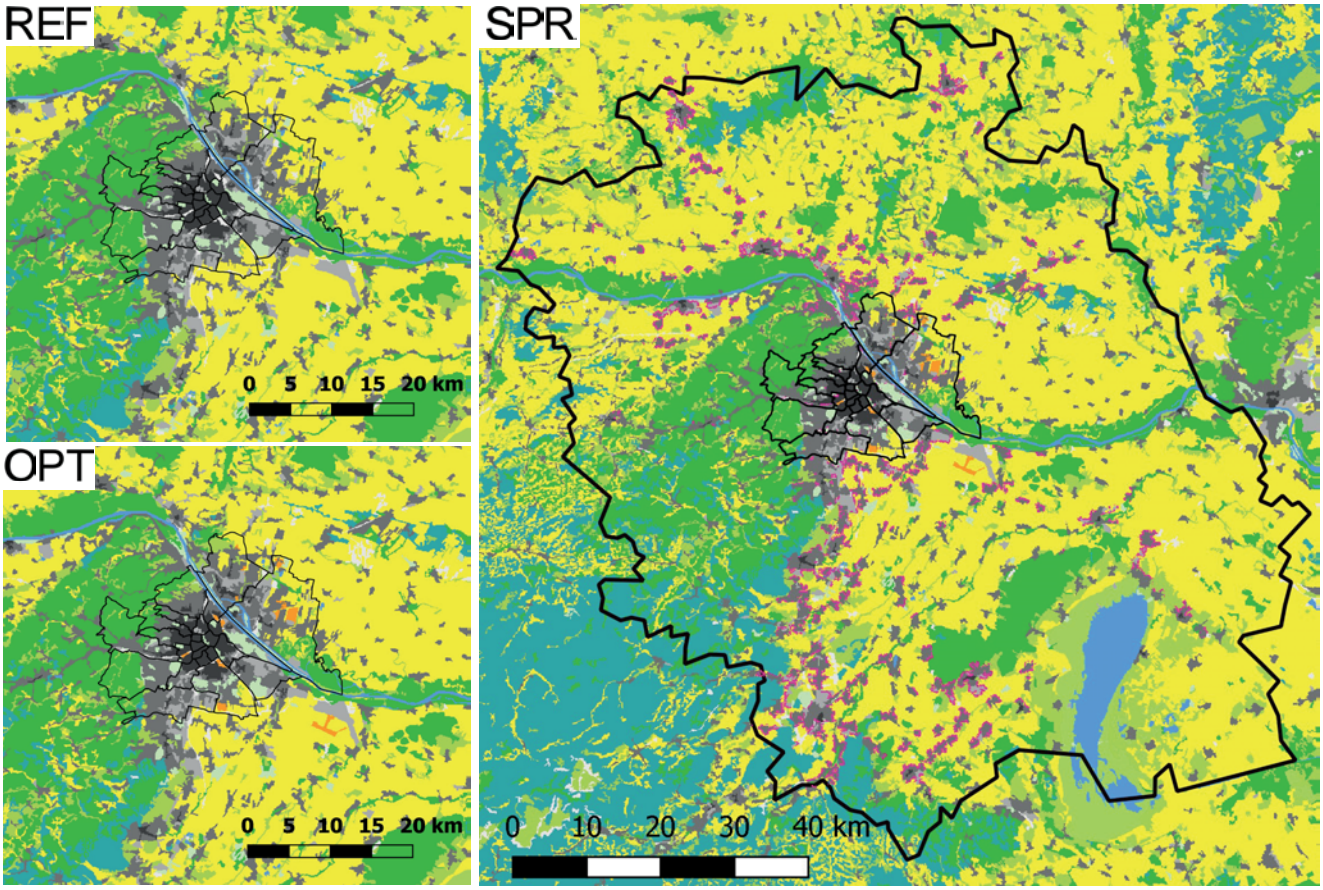

Figure 1: Spatial location of urban area in the three urban development scenarios: a) REF (up left), b) SPR (right) and c) OPT (down left). Actual urban areas are dark, middle and bright grey (high density residential, low density residential and commercial). Additional urban sprawl areas are purple. Known development areas are orange. Vegetation areas: yellow: dryland cropland and pasture (USGS class 2), bright green: mixed dryland/irrigated cropland and pasture (USGS class 4), brown-green: crops, shrubs, woodland mosaic (USGS classes 6+9), dark-green: deciduous forest (USGS class 11), blue-green: mixed forest (USGS class 15). The green areas surrounding the lake Neusiedel (south east of the region) is herbaceous wetland. The district borders of Vienna are thin black lines. The thick black line shows the border of stadtregion+ (PGO 2011).

The pre-1919 structure of Vienna is rather uniform, consisting of mainly brick, partly lime stone walls of about 50 cm thickness. They are not insulated, have double glazing windows and a steep roof constructions covered with clay bricks. The more recent buildings are more diverse regarding morphology as well as physical parameters related to building construction practices (e.g., the main wall material and insulation material).

The first measure consists of enhancing the building insulation. The thermal conductivity of the roof and walls is decreased to 0.1 W/mK, which is the nearly zero-energy standard and required for all new buildings after 2020 according to the Energy Performance of Buildings Directive EPBD (http://data.europa.eu/eli/dir/2018/844/oj; Amtmann and Altmann-Mavaddat, 2014). The thermal conductivity of windows is decreased to 0.9 W/mK, which is a typical value used in refurbishment of multistoried buildings (Amtmann and Altmann-Mavaddat, 2014). The thermal conductivity of roads is decreased to 0.4 W/mK, which is the lower boundary for medium concrete (https://www.engineeringtoolbox.com/thermal-conductivity-d_429.html). This change in material properties leads to a strong reduction of heat uptake by urban materials during the day, which is expected to cool the city during the evening, thus it might be an important factor for more effective cooling of rooms that have heated up. During the day, the well insulated urban structure is expected to take up less energy, which could lead to higher air temperatures during the day.

The second measure is intended to counteract the higher air temperature during the day due to the enhanced building insulation. The albedo of the walls and roads is only slightly increased from 0.2 and 0.13, respectively, to 0.3, which increases reflection of solar radiation, but also can help to reduce air temperatures (Krispel et al., 2017; Weihs et al., 2018). The albedo of the roof is increased to 0.68, which is technically possible and more effective in order to reduce sensible heat flux, as has been investigated in various studies (Taha et al., 1997; Morini et al., 2016; Žuvela-Aloise et al., 2018). Fallmann et al. (2016) showed further that such measures are not likely to have known negative effects on the boundary layer height and pollutant concentrations. The albedo increase mainly counteracts the increase in air temperature during sunlit hours. Therefore, all negative effects of decreased thermal conductivity should be mitigated. Ramamurthy et al. (2015) analyzed the effectiveness insulation and high reflective roofs with an urban canopy model and suggests a combination. We note that the increase in albedo values does not depend on water availability and space demands, but it does compete with available surface areas for photovoltaic and green roof surfaces.

2.4.2 Resilience measures

The different resilience measures used in the OPT scenario are simulated separately in order to allow for a precise attribution of their effect. In the following, the reduction of thermal conductivity is referred hereinafter as INS, the increase of albedo as ALB, and the densification caused by changes of built area from 0.22 (low residential areas) and 0.16 (commercial areas) to 0.242 as DEN. In addition, further potential mitigation and adaptation measures are investigated. These are a green roof (referred hereinafter as GRR) and a photovoltaic roof (referred hereinafter as PVR) scenario. For the GRR, the green roof module is used (De Munck et al., 2013). An extensive roof coverage using sedum is assumed. For PVR, the photovoltaic roof module is used (Masson et al., 2014) assuming an efficiency of 20 % and an albedo of 10 % for the solar panels. An overview of all employed scenarios is given in Table 1. All these measures are applied on 100 % of the roof surface, which is a first and rather extreme approximation to estimate the potential maximum effects of such resilience measures. Apart from being adaptation measures, which mitigate the urban heat island by reducing air temperatures by conversion of sunlight to either electric current or photosynthesis and evapotranspiration at roof level, PVR is an effective mitigative measure, which helps to avoid greenhouse gas emissions. Green roofs, as active soil and vegetation layer could help to mitigate high green house gas concentrations in the atmosphere as a carbon sink (Li and Babcock, 2014).

2.5 Present and future heat wave

An analysis of 15-yearly events is done in order to select suitable heat waves from external data that can be used to force the WRF simulations. The selected heat waves are 15 year return period events taken from the historical climate period (1988–2017, centred at 2002, "hw15yACT") and also a future climate period (2036–2065, centred at 2050, "hw15ySCE"). The selection is based on the average daily maximum 2 m air temperature of heat waves (5 days). The historical heat wave is selected using observational data at the station Wien Hohe Warte supplied by the Austrian weather service ZAMG. The 5 day average daily maximum air temperature is calculated for the last 30 years (1988 to 2017) and the return period of these 5 day events is estimated using the Generalized Extreme Value Distribution (GEV; Fisher and Tippett, 1928). Due to the strong positive trend of more than 2 K within the last three decades for daily maximum air temperature, the data are detrended before applying the GEV.

As a reference heat wave for present-day modelling we choose the most intense 5 day heat wave of 1988–2017, which occurred in summer of 2015 with a 5 day temperature maximum mean of 36.3 °C (Table 2). According to the GEV distribution this event represents a heat wave with a return period of 15 years.

The regional climate change scenarios are based on the ensemble ÖKS 15 (Leuprecht et al., 2017; BMNT, 2016), a selection of 26 regional climate model scenarios from EURO-CORDEX (Jacob et al., 2014), derived

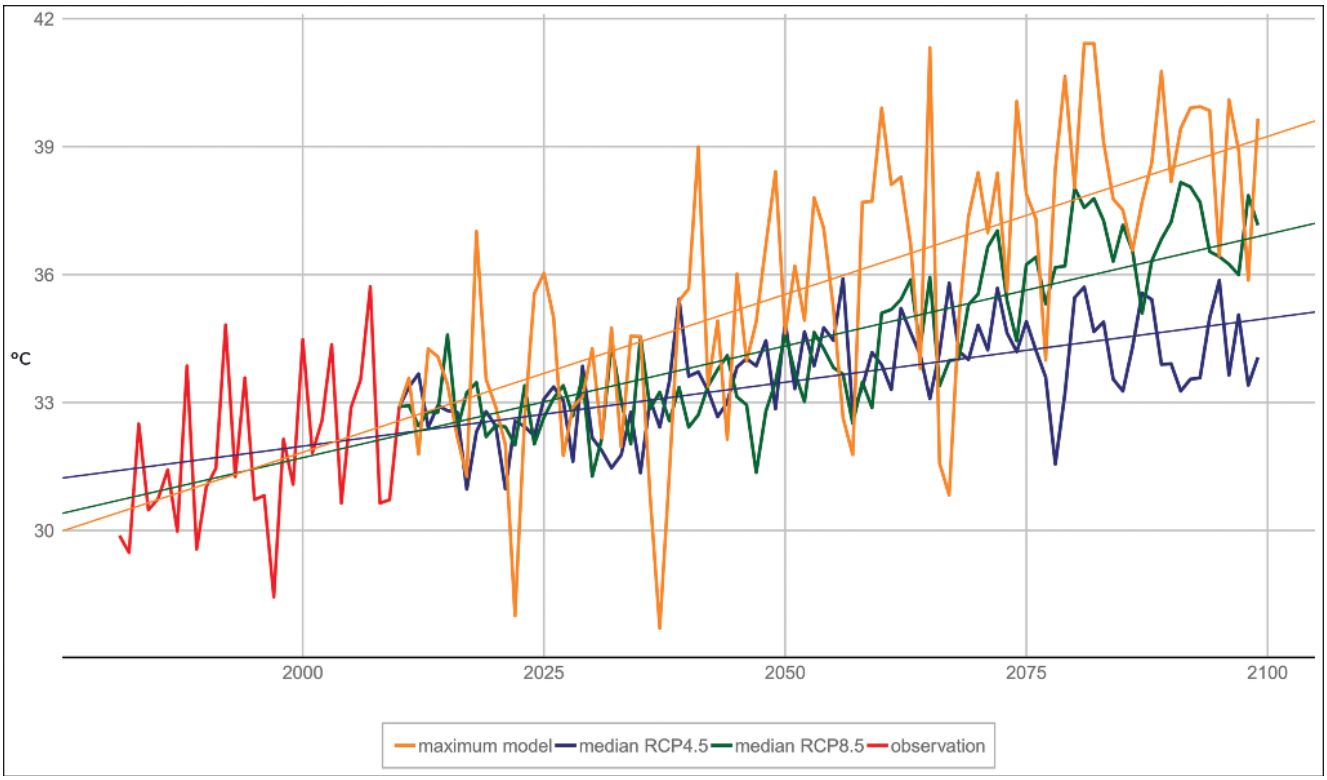

Figure 2: Maximum 5 day heat wave temperature (average of the daily temperature maximum of five consecutive days) per year at Vienna Hohe Warte observed (red), median of all scenarios forced with RCP4.5 (blue), median of all scenarios forced with RCP8.5 (green), scenario with the strongest trend of the whole ensemble (orange) and linear trend lines.

Table 2: Average daily maximum 2 m air temperature of heat waves (5 days) with 1, 2 and 15 year return periods derived from the station observations of Vienna Hohe Warte for the period 1988–2017 (first row) and climate change signals (2036–2065 versus 1988–2017) for this indicator based on the ÖKS 15 scenarios (Leuprecht et al., 2017) at a 1 km^2 grid cell at the same location.

Emission scenario/Return period	1 year	2 year	15 year
Observation (1988–2017) [°C]	28.7	31.6	36.3
RCP 4.5 ensemble median [K]	1.5	2.2	2.5
RCP 8.5 ensemble median [K]	1.8	2.7	2.2
Ensemble maximum [K]	5.9	3.7	4.8

from different global (Taylor et al., 2012) and regional climate models and forced with the emission scenarios RCP4.5 and RCP8.5. The ÖKS15 ensemble provides bias-corrected and localized (1 km) scenarios for daily minimum and maximum temperature, daily precipitation and daily radiation. Bias correction was done using a quantile mapping as described in Switanek et al. (2017). As only the daily maximum temperature is used for the quantification of the meteorological trend of the maximum temperature during 5 day heat waves, the spatial resolution of 1 km is sufficient.

For every ensemble member of ÖKS 15, we calculate the annual maximum 5-day mean of the daily maximum air temperature for the grid cell representing Hohe Warte in Vienna. Using the same GEV method we calculate the heat wave air temperature for return periods of 1, 2 and 15 year events for the historical period 1988–2017 and the future period of 2036–2065. In Fig. 2, the development of the maximum 5-day heat wave air temperature per year is shown for observations (red), the ensemble median of all scenarios forced with RCP4.5 (blue), RCP8.5 (green) and the scenario with the strongest trend in heat wave air temperature of the whole ensemble (orange).

The observed heat wave air temperature at Wien Hohe Warte for 1, 2 and 15 year events of the period 1988–2017 and the climate change signal until the middle of the 21st century is given in Table 2. There are no large differences for the ensemble means between the two emission scenarios until the middle of the century. For the 15 year event, the RCP4.5 ensemble shows even a 0.3 K stronger warming than RCP8.5. However, there is a more pronounced warming seen when the more extreme heat waves occur. The 1 year events show a warming between 1.5 and 1.8 K and the 2 and 15 year events have a warming between 2.2 and 2.7 K. For the ensemble maximum scenario this relation is not seen and the strongest warming is for the 1 year event.

For the selection of the future scenario we chose the historical 15 year event heat wave air temperature (36.3 °C) and added the climate change signal of the 15 year event from the most extreme scenario (4.8 K). This choice can be interpreted as a plausible worst case scenario until the middle of the 21st century. This ex-

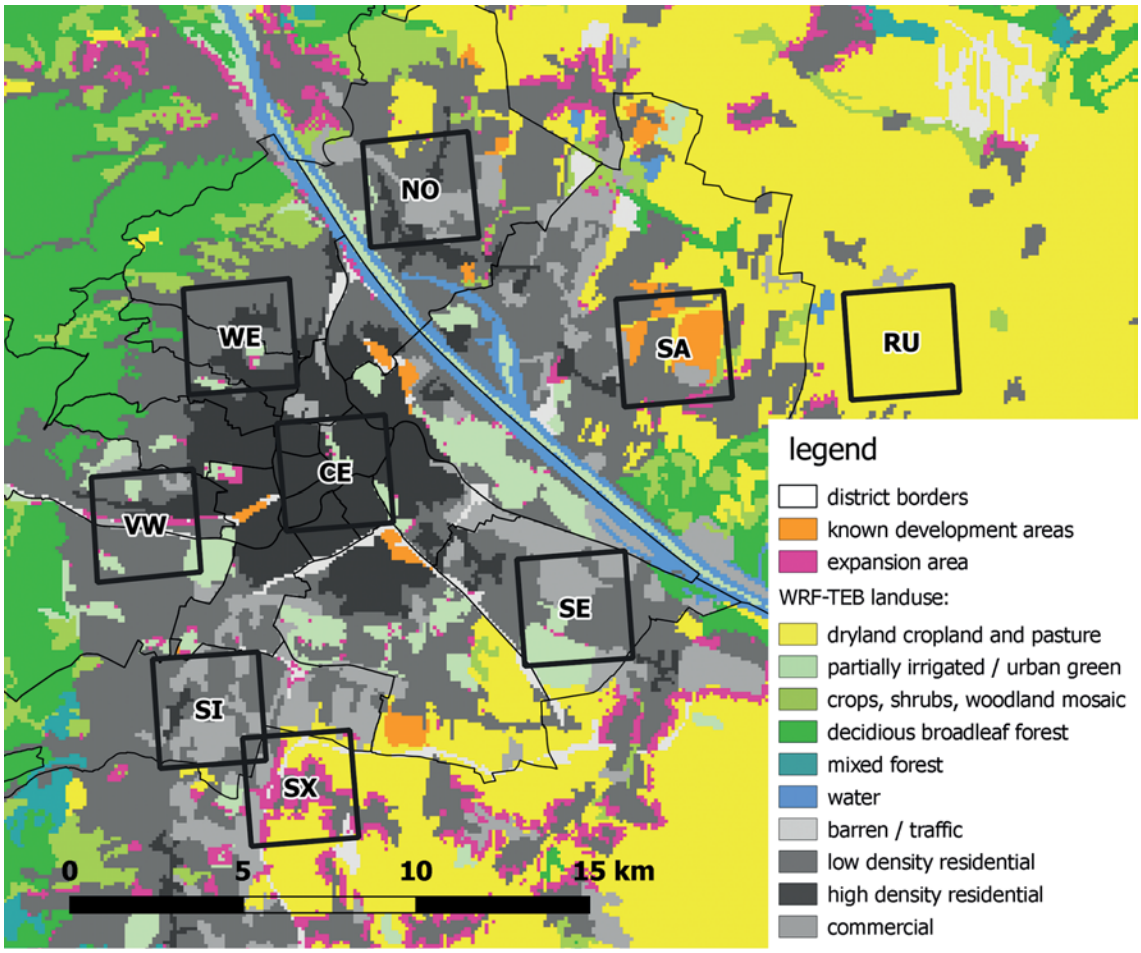

Figure 3: Subregions chosen for further analysis (clockwise): Central Districts (CE), North-Rim (NO), New development areas: Seestadt Aspern (SA), South-eastern rim (SE), South-industrial (SI), South expansion (SX), Valley of Wien (VW), West – elevated low density residential (WE), Rural area (RU).

Table 3: Mean values for Town Fraction (FRAC_TOWN) as they were calculated within this study, Built fraction [-] (D_BLD), Unsealed fraction [-] (D_GARDEN), Building height [m] (D_BLD_HEIG) and Vertical to horizontal wall factor [-] (D_WALL_O_H) for the Subregions of Fig. 3.

	CE	NO	RU	SA	SE	SI	SX	VW	WE
FRAC_TOWN	0.95	0.9	0.05	0.46	0.89	0.95	0.47	0.84	0.88
D_BLD	0.43	0.23	0.16	0.21	0.19	0.21	0.19	0.25	0.25
D_GARDEN	0.19	0.5	0.54	0.53	0.53	0.52	0.53	0.47	0.47
D_BLD_HEIG	18.75	11.44	11.2	10.68	10.9	11.13	10.85	12.11	11.85
D_WALL_O_H	1.75	1.11	0.5	1.08	0.83	1	0.89	1.2	1.27

treme climate scenario should also maximise the impact of the change of the urban structure (temperature increase) and should help to identify possible interactions between climate and land-use changes.

The lateral boundary conditions for a heat wave that fulfils the air temperature criteria (41.3 °C average 5 day daily maximum air temperature) are taken from a high-resolution regional climate scenario simulation. This simulation is based on the global model GFDL-CM3 (Donner et al., 2011) forced with the RCP8.5 emission scenario and downscaled with the WRF model (Michalakes et al., 2001) with an optimized set up for the Alpine region (Arnold et al., 2011). The regional model has a 10 km^2 spatial resolution and was run for the Alpine region and the whole 21st century. In addition to the 5-day period, a spin-up period of two–three days is used.

2.6 Study regions

For the presentation of the results, 9 areas of 9×9 model grid cells each (total of each area: 81 cells, 9 km^2) are chosen to represent the variety within Vienna (Fig. 3, Table 3). The main subregion covers the central districts.

The magnitude of the urban heat island is quantified by calculating the spatial mean difference in the daily minimum values in 2 m air temperature between the grid cells of the central districts subregion (CE) and the rural (RU) subregion. The new development areas around Seestadt Aspern (SA) are chosen to quantify the change caused by the erection of this new built urban area. North-Rim (NO), South-industrial (SI), South-eastern rim (SE), are chosen as areas with high industrial coverage, which is likely to be densified, but are in suburban areas in different cardinal directions and thus exposed to different wind regimes. South expansion (SE) is chosen as another suburban area where urban densification is unlikely but urban sprawl is likely. Furthermore, a subregion in the west-elevated low density residential (WE) was chosen as representative for the climatological situation in the areas influenced by the far reaching forested and hilly areas west of Vienna and without change in the land use. Finally, an area in the Valley of Wien (VW) shall give information about changes in this area, which is climatologically distinct due to a valley breeze.

3 Results

Two reference heat waves were run for present (hw15yACT) and future (hw15ySCE) conditions. They were selected by their air temperature value. They both have very low wind speeds during the night (1 m/s) – so there is hardly any air advected (Figure D-1). During the day the wind ranges between 3 and 4 m/s. For hw15yACT it is from East to Southeast, for hw15ySCE it is from East to Northeast (Figure D-1). There were some disturbances in the downward shortwave flux at the ground surfaces (Figure D-2). So, these days were excluded together with the spin up time. Consequently, for hw15yACT 9, 10, 12 and 13 August 2015 (day 4, 5, 7 and 8) is used. For hw15ySCE 7 and 8 July 2069 (day 7 and 8) is used. The minima and maximum values for 2 m air temperature, MRT, canyon air temperature and UTCI shade are calculated using all daily extremes of each of the 81 grid cells of the cloud free days of the selected period. For the present heat wave these are 324 values (4 days), for the future heat wave there are 162 values (2 days).

The air advected from either of these directions stems mainly from agricultural plains. The 2 m air temperature in these agricultural regions are rather uniform with spatial differences smaller than 1 K for hw15yACT and 2 K for hw15ySCE (Figure D-3). Also, the simulated humidity field is uniform with spatial deviations from less than 2 g kg^{-1} (Figure D-4). The future heat wave shows temperatures above 40 °C with a mixing ratio of 10 g kg^{-1} (mean water vapour pressure of 13.5 hPa). Both simulations have a surface pressure below 1000 hPa. For the present heat wave the dew point temperature did not surpass critical levels to cause sultriness. Also, for the future heat wave non-sultry conditions are expected. Soil moisture is declining near the surface during the heat wave (Figure D-5).

3.1 Viennese future heat load (T_{max}) and UHI (T_{min})

3.1.1 Reference scenario

The average daily maximum air temperature simulated by WRF-TEB (T_{max}) increases by about 7 K between the historical and future heat wave (Fig. 5). Simulated average daily minimum air temperature (T_{min}) increases between 2 and 4 K (Fig. 5). In the central districts the mean increases are 6.7 K and 3.2 K, respectively. The median values are slightly higher (6.8 K and 3.4 K). The variation of T_{min} between the different areas is higher than that of T_{max}. The urban-rural difference of the T_{min} between Vienna city centre (CE) and the eastern agricultural areas (RU) for the present heat wave is 3.0 K. For the future heat wave, the urban-rural difference is greatly increased to 4.6 K (Fig. 4, 5, 6).

3.1.2 Future urban scenarios

The urban scenarios show a larger effect on minimum than on maximum air temperature (Fig. 5, 6). The influence on air temperature is generally less than 1 K, which is low compared to the air temperature increase due to climate change projected by the climate models (Fig. 5, 6). While SPR increases T_{min}, OPT decreases T_{min} for hw15yACT (Fig. 4 upper middle and right) and for hw15ySCE (Fig. 6). For SPR, the T_{max} changes less than 0.1 K (Fig. 5). For OPT, the T_{max} decreases in the range of 0.5 K for the subregions CE, SI, SX, VW and WE (Fig. 5).

3.2 Effects of resilience measures

The components of the OPT scenario (ALB, INS, DEN) as well as GRR and PVR are further analyzed.

First, the general influence on the town heat fluxes is shown for CE (3.2.1). Then the surface temperature of roof, ground and wall show more information (3.2.2).

3.2.1 Town energy fluxes in the central districts

At daytime for the ALB scenario, a reduction of up to 180 W/m^2 in net radiation and of about 100 W/m^2 in sensible heat flux is simulated. The effects are relatively constant throughout the heat wave (Fig. 7a). The INS scenario shows during the day on the one hand a decrease of the ground heat flux up to 150 W/m^2, but an increase of the same magnitude of the sensible heat flux. During nighttime, the sensible heat flux is decreased up to 100 W/m^2 (Fig. 7b) and thus also air temperature is lower at night. The change in energy balance is mainly negative, with a declining trend. Also, the difference of sensible heat flux during the day shows a declining trend towards the end of the heat wave. For the DEN scenario, the ground heat flux increases by 100 W/m^2 during the day and decreases by 30 W/m^2 during the night (Fig. 7c). The implementation of green roofs (GRR) increases net radiation by up to 80 W/m^2 during the day – an effect

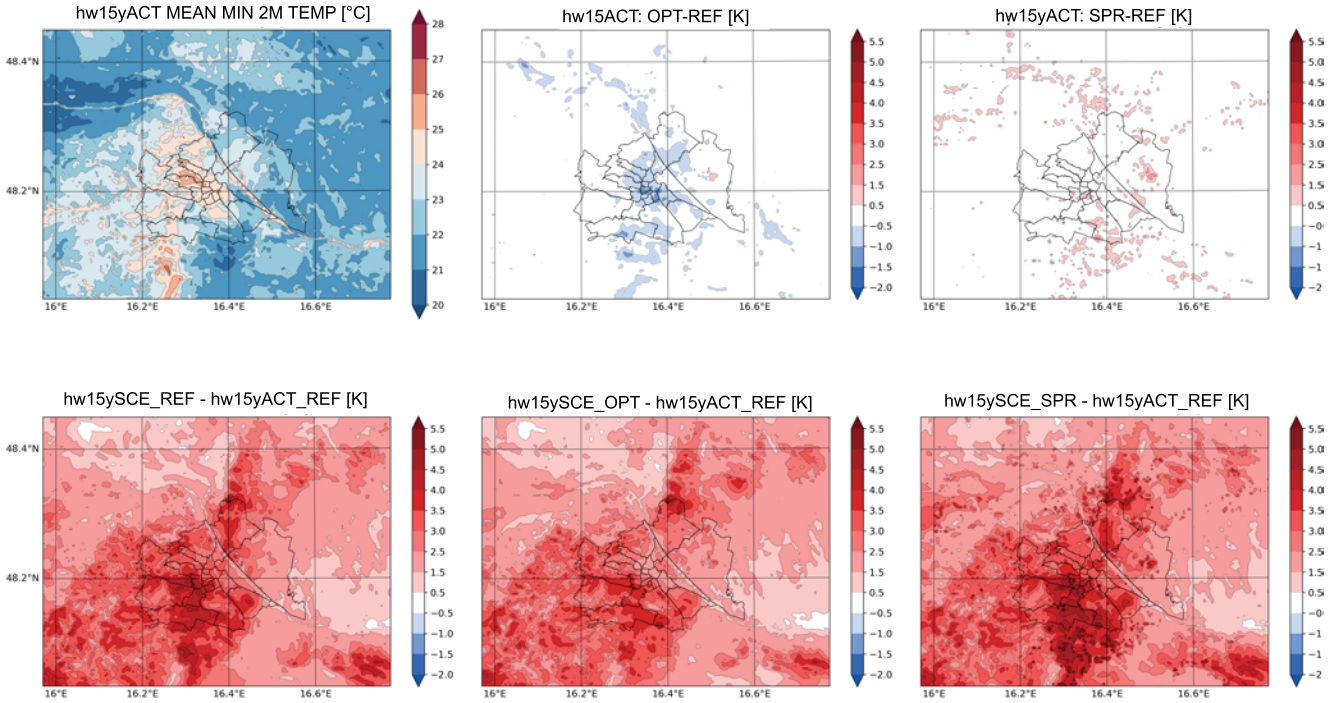

Figure 4: Mean minimum of the selected cloud free days for each grid cell for the daily 2 m minimum air temperature for the present heat wave hw15yACT (upper left). Differences between reference scenario hw15yACT and urban development scenarios OPT (middle) and SPR (right) (upper panels). Differences between reference scenario for present (hw15yACT) and future (hw15yrSCE) for the REF (left), OPT (middle) and SPR (right) urban development scenario (lower panels).

that diminishes to the end of the heat wave (Fig. 7d). The latent heat flux increases by up to 230 W/m^2, the sensible heat flux decreases by up to 100 W/m^2. The implementation of solar panels (PVR) decreases both the sensible heat flux and the net radiation by about 100 W/m^2 (Fig. 7e).

3.2.2 Surface temperatures of roof, wall and road in the central districts

On the roof five resilience measures show different properties. This causes a different increase in roof surface temperature during the day (Fig. 8a). The strongest diurnal amplitude is seen in INS. GRR and ALB both have cooler roof surfaces than REF. PVR stays coolest under the assumptions of this study.

The surfaces within the canyon are only altered in ALB and INS, therefore only these resilience measures are shown for wall and road. On the unsealed fraction there are no changes done. The wall surfaces show that INS strongly alters the wall surface temperature compared to REF. During daytime, there is an increase by more than 10 K and during night a decrease of up to 5 K (Fig. 8b).

The road surface temperatures show the least changes, but also here it can be seen that INS increases the maximum surface temperature whereas ALB decreases it (Fig. 8c).

3.3 Canyon parameters and human thermal stress

Finally, the parameters relevant to quantify human thermal stress or comfort are analyzed within the street canyon. For the canyon wind speed no changes greater than 0.5 m/s have been found. Also, the canyon humidity changes are $\ll$ 0.01 kg/kg. For the MRT and canyon air temperature there do exist notable changes. During heat waves after MRT, the air temperature has a great impact on determining whether the UTCI reaches thermal stress levels or stays in the human thermal comfort region. Therefore, the effect of the separate measures on the mean radiant temperature and canyon air temperature was analyzed. In Fig. 9 timeseries of MRT and canyon air temperature during the whole heat wave hw15ySCE are shown for the central districts (CE). Table 4, 5 and 5 give additional information about the minima and maxima in the subregions.

3.3.1 MRT

The MRT maxima for the reference scenario increase by 6.6 K in the shade and 7.6 K in the sun between the present and future scenario for the central districts (Table 4a). For GRR, DEN and PVR the difference in MRT maxima to the reference scenario was less than 0.2 K (Table 4b, 4c) for all subregions. For ALB the mean increase of maximum MRT is 2.3 (Table 4c, Fig. 9a) for CE. For INS the MRT increased during day up to 8 K

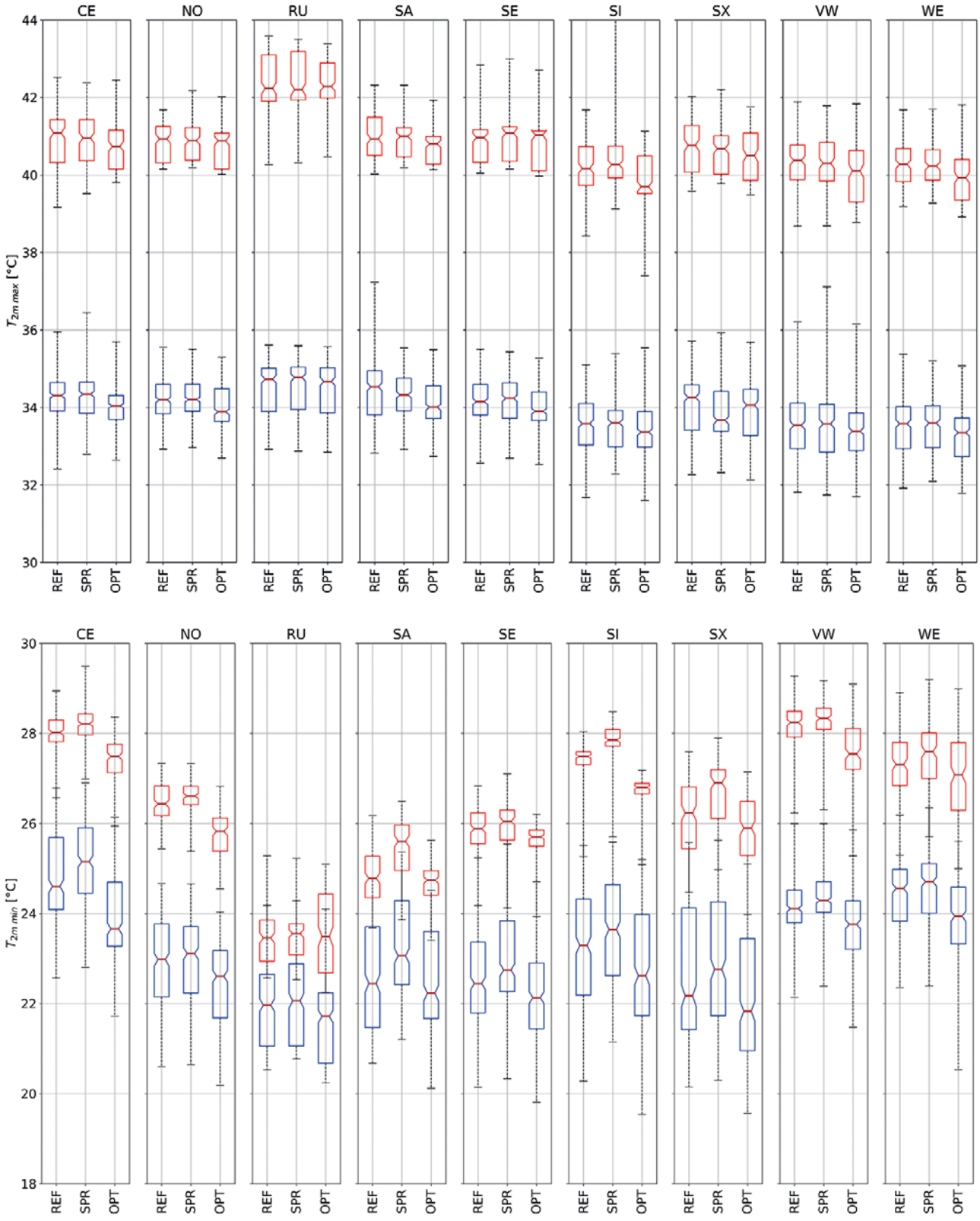

Figure 5 and 6: 2 m air temperature for the selected cloud free days of the chosen climate episode for present (hw15yACT, blue) and future (hw15ySCE, red) and the 3 different urban development scenarios (sh. Table 1) for daily maximum temperature (above) and daily minimum temperature (below) in the 9 different subregions (Fig. 3): Central Districts (CE), North-Rim (NO), New development areas: Seestadt Aspern (SA), South-eastern rim (SE), South-industrial (SI), South expansion (SX), Valley of Wien (VW), West – elevated low density residential (WE), Rural area (RU).

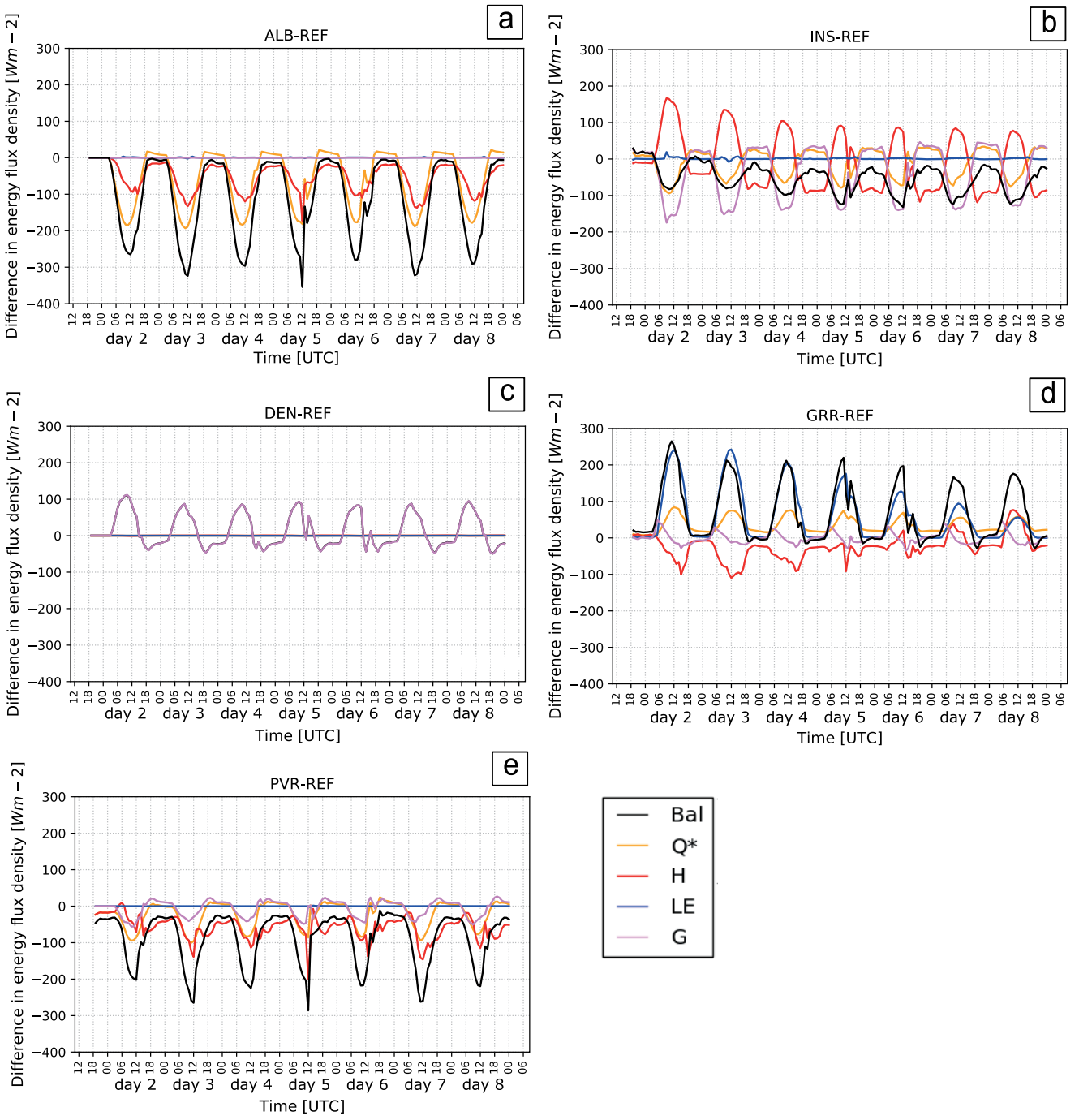

Figure 7: Timeseries differences compared to reference (REF) of radiation balance (Q*), sensible (H), latent (LE) (positive downwards), ground (G) heat flux and energy balance (Bal) during the hw15ySCE in the Central Districts (CE) for different measures: ALB (increased albedo), INS (insulation), DEN (density), GRR (green roof) and PVR (photovoltaic roof)

and decreased at night up to 3 K (Fig. 9b) for CE. On average this is an increase of 5 K (Table 4c) for CE. Both the daily maxima and minima of both variables show a declining trend for CE (Fig. 9b).

3.3.2 Canyon air temperature

For SPR the maximum canyon air temperature increases by 0.2 K (Table 5b) in the central districts (CE). For OPT, both the minimum and maximum canyon temperature decrease by 0.2 and 0.9 K in CE (Table 5b, 5c) respectively. In the new urbanized areas (SA) itself the maximum and minimum canyon temperature increase by 0.7 and 1.0 K for SPR. In the OPT scenario, the mean increase is only 0.5 K and 0.3 K in SA (Table 5b, 5c) while for the median of the 2 m air temperature calculated by WRF-TEB there is even a decrease (Fig. 5 and 6).

For ALB the canyon air temperature maxima and minima decrease by not more than 0.2 K and 0.1 K, respectively in all subregions (Table 5b, 5c). For INS

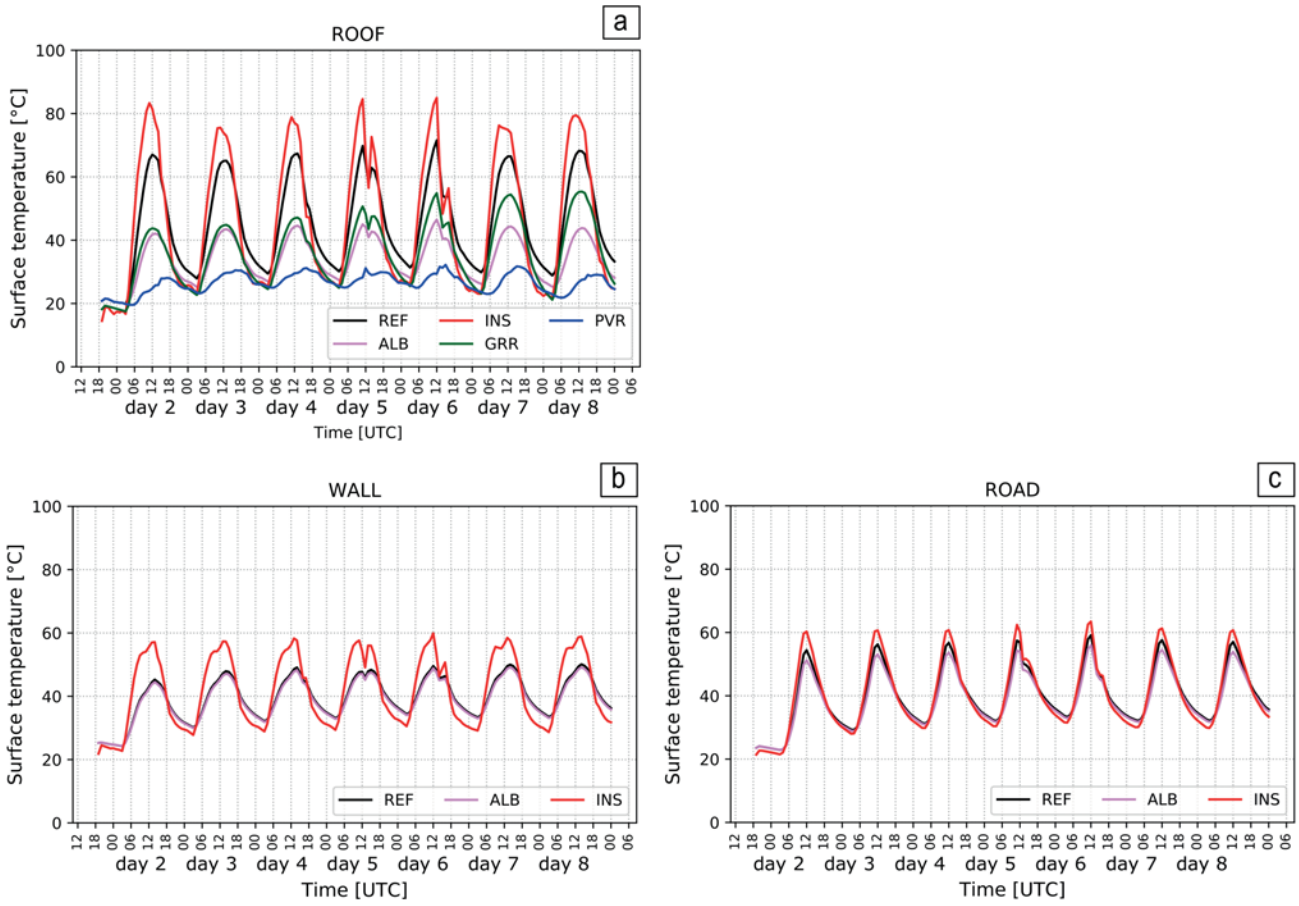

Figure 8: Time series of the surface temperature of roof (a), wall (b) and road (c) of the resilience measures where changes have been applied to these surfaces – during the future episode (hw15ySCE) for the Central Districts (CE).

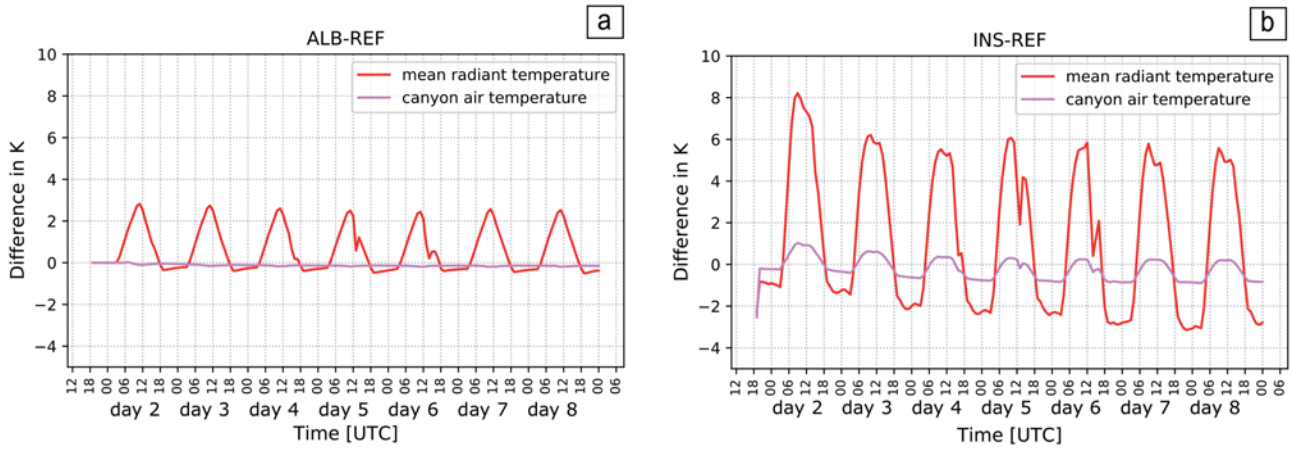

Figure 9: Difference of time series of two elements of UTCI, changed by the resilience measures: Mean radiant temperature in the shade and canyon air temperature during the future episode (hw15ySCE) for the Central Districts (CE).

the maximum canyon temperature does not increase by more than 0.1 K while the minimum canyon temperature decreases up to 0.8 K, where 0.8 K are only reached in the central districts (Table 5b, 5c). For DEN the changes for maximum and minimum canyon air temperature are below 0.1 K in all subregions (Table 5b, 5c). For GRR both maximum and minimum canyon air temperature decrease by 0.1 K and 0.2 K, respectively, in CE and are lower in all other subregions (Table 5b, 5c). For PVR both maximum and minimum canyon air temperature decrease by 0.2 K and 0.2 K in CE and are lower in all other subregions (Table 5b, 5c), respectively.

Table 4: a) absolute maximum and minimum radiant temperature (MRT) values [°C] of the actual (hw15yACT – "ACT") and future heat wave (hw15ySCE – "SCE") of the reference run and differences [K] of b) maximum MRT in the sun c) maximum MRT in the shade and d) minimum MRT (shade = sun) to the reference run hw15ySCE for the cloud free days of the selected episode, for all urban scenarios and *resilience measures* spatial mean in the 9 different subregions (Fig. 3): Central Districts (CE), North-Rim (NO), New development areas: Seestadt Aspern (SA), South-eastern rim (SE), South-industrial (SI), South expansion (SX), Valley of Wien (VW), West – elevated low density residential (WE), Rural area (RU) – which is *only based on 4 values. Differences over +/−1 are marked red/blue.

a) MRT		CE	NO	RU*	SA	SE	SX	SI	VW	WE
REF ACT	Shade, max	47.8	50.8	50.4	51.9	50.9	51.3	51.0	50.5	50.7
REF ACT	Shade, min	27.5	23.6	20.2	23.2	22.3	22.6	23.2	24.1	24.7
REF ACT	Sun, max	73.2	75.9	75.2	76.5	75.8	76.2	76.1	75.6	24.8
REF SCE	Shade, max	54.4	56.6	54.2	57.07	56.0	55.1	55.4	55.8	56.1
REF SCE	Shade, min	30.9	25.9	21.1	25.16	24.2	24.6	25.8	27.3	27.4
REF SCE	Sun, max	80.8	82.4	80.6	82.73	81.9	81.4	81.7	81.9	82.1
b) maximum MRT in the sun, differences to REF (both: hw15ySCE)										
SPR		−0.1	−0.1	0.3	−0.9	0.1	0.3	0.2	0.0	0.0
OPT		0.6	0.2	0.5	−0.5	0.4	0.5	0.5	0.4	0.6
ALB		*1.9*	*1.5*	*1.6*	*1.4*	*1.5*	*1.6*	*1.6*	*1.6*	*1.6*
INS		*4.0*	*2.3*	*1.3*	*2.2*	*1.9*	*1.6*	*1.8*	*2.2*	*2.4*
DEN		*0.0*	*0.1*	*0.1*	*0.0*	*0.1*	*0.1*	*0.1*	*0.1*	*0.1*
GRR		*−0.1*	*−0.0*	*−0.0*	*−0.0*	*−0.0*	*−0.0*	*−0.0*	*−0.1*	*−0.1*
PVR		*−0.1*	*−0.1*	*−0.0*	*−0.1*	*−0.1*	*−0.1*	*−0.1*	*−0.1*	*−0.1*
c) maximum MRT in the shade, differences to REF (both: hw15ySCE)										
SPR		−0.1	−0.1	0.6	−1.3	0.1	0.5	0.3	0.1	0.1
OPT		0.3	−0.1	0.6	−1.1	0.2	0.4	0.6	0.3	0.50
ALB		*2.3*	*1.8*	*2.0*	*1.8*	*1.8*	*1.9*	*1.9*	*2.0*	*1.9*
INS		*5.0*	*3.0*	*1.7*	*2.8*	*2.6*	*2.0*	*2.3*	*2.8*	*3.0*
DEN		*0.0*	*0.1*	*0.1*	*0.0*	*0.1*	*0.1*	*0.1*	*0.1*	*0.1*
GRR		*−0.1*	*−0.1*	*−0.0*	*−0.1*	*−0.0*	*−0.0*	*−0.1*	*−0.1*	*−0.1*
PVR		*−0.2*	*−0.1*	*−0.0*	*−0.1*	*−0.1*	*−0.1*	*−0.1*	*−0.1*	*−0.1*
d) minimum MRT, differences to REF (both: hw15ySCE)										
SPR		0.0	0.2	0.1	2.2	0.1	0.8	0.1	0.1	0
OPT		−0.4	0.2	0.2	2.3	0.3	0.2	0.1	0.2	0.3
ALB		*−0.3*	*−0.3*	*−0.2*	*−0.2*	*−0.3*	*−0.3*	*−0.3*	*−0.3*	*−0.3*
INS		*−3.1*	*−2.6*	*−1.9*	*−2.6*	*−2.5*	*−2.5*	*−2.6*	*−2.6*	*−2.8*
DEN		*0.0*	*0.5*	*0.4*	*0.6*	*0.5*	*0.5*	*0.5*	*0.5*	*0.5*
GRR		*−0.2*	*−0.1*	*−0.1*	*−0.1*	*−0.1*	*−0.1*	*−0.1*	*−0.1*	*−0.1*
PVR		*−0.2*	*−0.1*	*−0.1*	*−0.1*	*−0.1*	*−0.1*	*−0.1*	*−0.1*	*−0.1*

3.3.3 Universal Thermal Comfort Index (UTCI)

Both MRT and canyon air temperature influence the magnitude of UTCI. Here, mainly UTCI shade is used. The maximum future UTCI in the sun for hw15ySCE is included as reference in Table 6e. Values of 51.0 °C in the central districts (CE) and 49.6 °C in the rural region (RU) are extremely heat stressed (Bröde et al., 2012), so that we did not think it feasible to reduce it to a comfortable range by applying resilience measures. Between the present (hw15yACT) and future (hw15ySCE) heat wave there is already an increase of 5.3–6.3 K for the absolute maximum UTCI shade averaged over the different subregions (Table 6a). The absolute minimum UTCI changes least in the rural areas, but within the urban areas can increase up to 3 K (Table 6c).

Compared to the reference scenario (REF), in the urban sprawl scenario (SPR), the UTCI increases excluding SA (maximum UTCI by less than 0.1, minimum UTCI by up to 0.4), whereas in the optimized urban development scenario (OPT), the UTCI is reduced (maximum by up to 0.2 K, and the minimum by up to 0.7 K) in most areas. The largest differences are simulated in the new development areas (SA) where new urban districts are constructed on formerly unbuilt land (Table 6b, 6d). Here also in the OPT scenario there are increases of maximum and minimum UTCI by 0.9 K and 0.4 K, respectively. In the SPR scenario in the new development areas (SA) the UTCI maximum increases by 0.6 K and the minimum by 1.3 K. Also, in other areas of potential spread of settlement area, especially the minimum UTCI is increased, e.g., in South expansion areas (SX) by 0.4 K (Table 6d).

For ALB the average daily maximum UTCI increases by 0.2 K, while the average daily minimum decreases by 0.1 K in CE (Table 6b, 6d). For INS the daily maximum UTCI increases by 1.2 K, while the daily minimum decreases by 1.2 K in CE (Table 6b, 6d).

Table 5: a) absolute maximum and minimum canyon air temperature values [°C] of the future heat wave (hw15ySCE) for the reference run. b) differences [K] for the maximum canyon air temperature and c) differences [K] for the minimum canyon air temperature to the reference run hw15ySCE. average values for the cloud free days of the selected episode for all urban scenarios and *resilience measures* spatial mean in the 9 different subregions (Fig. 3): Central Districts (CE), North-Rim (NO), New development areas: Seestadt Aspern (SA), South-eastern rim (SE), South-industrial (SI), South expansion (SX), Valley of Wien (VW), West – elevated low density residential (WE), Rural area (RU) – which is *only based on 4 values. Differences over +/−0 0.25 are marked red/blue.

a) canyon air temperature	CE	NO	RU*	SA	SE	SX	SI	VW	WE
REF max	43.8	42.6	42.2	42.3	42.3	42.2	42.1	42.3	42.1
REF min	29.9	27.4	24.2	25.9	26.5	27.5	28.3	29.3	28.2
b) maximum canyon air temperature, differences to REF (both: hw15ySCE)									
SPR max	−0.0	−0.0	−0.0	0.7	0.1	0.1	−0.0	0	0.0
OPT max	−0.2	−0.1	−0.3	0.5	0.1	−0.2	−0.1	−0.2	−0.1
ALB max	*−0.2*	*−0.1*	*−0.1*	*−0.1*	*−0.1*	*−0.1*	*−0.2*	*−0.1*	*−0.1*
ISO max	*0.1*	*0.1*	*0.0*	*0.1*	*0.1*	*0.1*	*0.0*	*0.1*	*0.1*
DEN max	*0*	*0.0*	*−0.0*	*0.0*	*0.0*	*0.0*	*0.1*	*0.0*	*0.1*
GRR max	*−0.1*	*−0.0*	*−0.0*	*−0.0*	*−0.0*	*−0.0*	*−0.0*	*−0.0*	*−0.1*
PVR max	*−0.2*	*−0.1*	*−0.0*	*−0.0*	*−0.1*	*−0.1*	*−0.0*	*−0.1*	*−0.1*
c) minimum canyon air temperature, differences to REF (both: hw15ySCE)									
SPR min	0.2	0.3	0.2	1.0	0.0	0.3	0.3	0.1	0.2
OPT min	−0.9	−0.8	−0.1	0.3	−0.1	−0.3	−0.7	−0.8	−0.5
ALB min	*−0.1*	*−0.1*	*−0.1*	*−0.1*	*−0.1*	*−0.1*	*−0.1*	*−0.1*	*−0.1*
ISO min	*−0.8*	*−0.3*	*−0.0*	*−0.3*	*−0.3*	*−0.3*	*−0.3*	*−0.3*	*−0.3*
DEN min	*0.0*	*0.1*	*0.1*	*0.1*	*0.1*	*0.1*	*0.1*	*0.1*	*0.0*
GRR min	*−0.2*	*−0.1*	*−0.1*	*−0.1*	*−0.1*	*−0.0*	*−0.1*	*−0.1*	*−0.1*
PVR min	*−0.2*	*−0.1*	*−0.1*	*−0.1*	*−0.1*	*−0.1*	*−0.1*	*−0.1*	*−0.1*

For DEN the changes of UTCI of both maxima and minima are below 0.1 K on average in the central districts, where no densification takes place. In the densified districts with widespread commercial/industrial areas (SE, SI and NO), canyon air temperature is increasing, but changes are still below 0.1 K. The daily maximum UTCI increases only below 0.1 K whereas the daily minimum UTCI increases by 0.2 K (Table 6b, 6d). For GRR the daily maximum UTCI decreases by 0.1 K whereas the daily minimum UTCI decreases by 0.2 K (Table 6b, 6d) in CE. For PVR the daily maximum UTCI decreases by 0.2 K and the daily minimum UTCI by 0.2 K (Table 6b, 6d) in CE.

Most scenarios show a significant difference to the reference in their extreme values with $p \ll 0.05$ using the T-Test for related samples in the central districts. Only SPR does not show a significant difference in minima and maxima UTCI when the central districts are compared.

4 Discussion

4.1 Global climate change and influence on the Vienna region

4.1.1 Air temperature (T_{max} and T_{min}):

The lateral boundary conditions of the future heat wave are taken from regional climate scenarios, which are based on the global model GFDL-CM3 (Donner et al., 2011) forced with the RCP8.5 emission. The air temperature calculated for the selected 9 km^2 subregions of Vienna using 3 nests in this study increases by up to 7 K for the T_{max} and 2 to 4 K for the T_{min} values from the heat waves hw15y2015ACT to hw15ySCE. This means that both heat waves have Kyselý days (Kyselý et al., 2000) and tropical nights (T_{min}>20 °C). This shows a strong increase in T_{max} for extreme heat waves compared to the mean annual air temperature increase of 3.5 K published by APCC (2014) and Gobiet et al. (2014), which also refers to A1B instead of the more extreme RCP8.5. For France increases of 6–13 K for different regions by 2100 have been projected by Bador et al. (2017). Seneviratne et al. (2018) found positive air temperature anomalies of 8 K for Central Europe for the 21st century. Soil moisture – temperature feedbacks after early and intensified depletion of root-zone soil moisture contribute significantly to the Central European strong increases in extreme temperature (Vidale et al., 2007; Vogel, 2018).

It is interesting to note that the projected increase in T_{max} (Fig. 5) is more than twice as strong as the increase projected for the mean annual temperature in Austria (3.5 K), while the T_{min} (Fig. 5) are projected to increase about the amount of the mean annual temperature. As a result, the daily temperature range is projected to increase. Such an increase in daily temperature range was also found by Cattiaux et al. (2015) and be could also be partly attributed to the decreasing surface evaporation due to soil moisture depletion in future European summers (Jasper et al., 2006). This also affects the ru-

Table 6: a) absolute maximum UTCI shade values [°C] of present (hw15yACT – cloud free days: 4, 5, 7, 8) and future (hw15ySCE – cloud free days: 7, 8) of the reference run followed by the difference [K] between the two heat waves and b) differences [K] to the reference run hw15ySCE average values for the cloud free days of the selected episode for all urban scenarios and *resilience measures* spatial mean in the 9 different subregions (Fig. 3): Central Districts (CE), North-Rim (NO), New development areas: Seestadt Aspern (SA), South-eastern rim (SE), South-industrial (SI), South expansion (SX), Valley of Wien (VW), West – elevated low density residential (WE), Rural area (RU). Differences over +/−0.5 are marked red/blue. c) and d) show the same for minimum UTCI shade, e) shows absolute maximum UTCI sun values for the hw15ySCE.

a) max UTCI shade	CE	NO	RU	SA	SE	SX	SI	VW	WE
hw15yACT	38.9	38.8	38.1	38.2	38.2	38.3	38.7	38.6	38.3
hw15ySCE	45.2	44.4	43.9	44.2	44.2	43.7	44.0	44.1	44.0
hw15ySCE-hw15yACT	6.3	5.6	5.8	5.6	6.0	5.4	5.3	5.5	5.7
b) max UTCI shade, differences to REF (both: hw15ySCE)									
SPR max	0.0	0.0	0.1	0.6	−0.1	0.1	−0.2	0.1	−0.0
OPT max	−0.1	−0.1	−0.0	0.4	−0.1	−0.0	−0.2	−0.1	0.2
ALB max	*0.2*	*0.3*	*0.2*	*0.3*	*0.3*	*0.3*	*0.3*	*0.3*	*0.3*
INS max	*1.2*	*0.8*	*0.3*	*0.6*	*0.6*	*0.5*	*0.5*	*0.7*	*0.7*
DEN max	*0.0*	*0.0*	*0.0*	*0.1*	*0.0*	*0.0*	*0.1*	*0.1*	*0.1*
GRR max	*−0.1*	*−0.0*	*0.5*	*0.1*	*−0.0*	*−0.0*	*−0.1*	*−0.0*	*−0.0*
PVR max	*−0.2*	*−0.1*	*0.5*	*0.0*	*−0.1*	*−0.0*	*−0.1*	*−0.1*	*−0.1*
c) min UTCI shade	CE	NO	RU	SA	SE	SX	SI	VW	WE
hw15yACT	26.6	23.5	21.7	23.3	22.0	23.1	23.9	24.4	25.3
hw15ySCE	28.8	25.8	22.1	24.5	24.9	25.4	26.4	27.4	26.9
hw15ySCE-hw15yACT	2.2	2.3	0.4	1.2	2.9	2.3	2.5	3.0	1.6
d) minimum UTCI shade, differences to REF (both: hw15ySCE)									
SPR min	0.2	0.3	0.3	1.3	0.0	0.4	0.2	0.1	−0.1
OPT min	−0.7	−0.5	0.1	0.9	0	−0.3	−0.6	−0.6	−0.4
ALB min	*−0.1*	*−0.1*	*−0.0*	*−0.0*	*−0.0*	*−0.1*	*−0.1*	*−0.1*	*−0.1*
INS min	*−1.2*	*−0.9*	*−0.8*	*−1.0*	*−0.7*	*−0.9*	*−0.8*	*−1.0*	*−0.8*
DEN min	*0.0*	*0.2*	*0.2*	*0.2*	*0.2*	*0.2*	*0.2*	*0.2*	*0.2*
GRR min	*−0.2*	*−0.1*	*−0.1*	*−0.1*	*−0.1*	*−0.1*	*−0.1*	*−0.1*	*−0.1*
PVR min	*−0.2*	*−0.1*	*−0.1*	*−0.1*	*−0.1*	*−0.1*	*−0.1*	*−0.1*	*−0.1*
e) maximum UTCI sun, absolute values									
hw15ySCE	51.0	50.3	49.5	50.0	50.0	49.4	49.7	49.8	49.8

ral surroundings, which are even more affected by reduced soil moisture than urban areas with high sealing fractions. Dryer soils have a lower heat capacity and can cool more strongly than wetter soils. Also, in this study a decrease of soil moisture was simulated (Figure D-5). This can explain the high values of T_{max} in the rural subregion during day but also the low values of T_{min} during night, thus this could be the reason of the increase of the future nocturnal urban-rural difference.

The nocturnal canopy UHI is expected to increase from 3 to 4.6 K which is caused rather by the lower increase of minimum temperatures in the rural areas than within the city.

The actual and future UHI is strongly dominated by the mesoscale thermal regime and especially the future UHI is affected by high temperature reinforced by dry fields in the surroundings, which is a known process during heat waves (Fischer and Seneviratne, 2007; Hartmann, 1994). Fischer and Seneviratne (2007) analyzed the interactions between soil moisture and atmosphere for the 2003 summer heat wave in Europe and found that precipitation deficits, early vegetation growth and positive radiation anomalies preceding the heat wave contributed to rapid loss of soil moisture. Zampieri et al. (2009) showed that drought in the Mediterranean region can favour heat waves conditions in Europe at a continental scale by change in atmospheric circulation and hot air mass advection. This would suggest, that soil moisture deficits ought to be reduced by suitable methods on a continent-scale rather than only regional scale. Duchez et al. (2016) and Kornhuber et al. (2017) name a stationary jet stream position, caused by global scale circulation patterns, that coincides with observed European temperature extremes, including the 2015 event.

4.1.2 Thermal comfort index UTCI

The Universal Thermal Climate Index (UTCI) is used by meteorological services to quantify outdoor human thermal comfort and has been included in TEB to provide standardized information about human thermal comfort for grid resolutions > 100 m and with highly parameterized building morphology. It takes into account whole body thermal effects thanks to a multi-node thermophysiological model. It is derived by the air temperature, water vapour pressure and MRT, which is a quantity that

describes the shortwave and longwave radiation balance of the human body at 2 m and wind speed at 10 m height (Jendritzky et al., 2012; Weihs et al., 2012). In this study first WRF-TEB uses the different urban roughness of the three used building morphologies to calculate a 10 m wind, which is 10 m above the mean building height – so around 30 m agl in the city centre. Within the UTCI calculation a 6th order polynomial is used that assumes a uniform roughness length of 0.01 and a logarithmic profile, which reduces the 10 m wind to 70 % at 1.3 m. Although the roughness length is low this attenuation is very similar to the attenuation between above roof and within canyon wind speeds presented in Erell et al. (2011), which is based on Pearlmutter et al. (2005). They found an attenuation of around 60 % and 70 % caused by street canyons of a height/width ratio 0.66 and 1.0, as they are common in the Viennese city structure, which varies +/−10 % dependent on the wind direction or 'angle of attack'. The influence of the low roughness was further calculated by first applying the Hellman's exponential law (Urban and Kysely, 2014; Ketterer et al., 2017) with the maximum roughness assumed for Vienna (z0 = 2) to calculate a more realistic reduction of wind speed from the 10 m level to 1.3 agl. Using this second approach the average wind speeds occurring in heat waves analysed in this study of 2.2 m/s were reduced to 0.3 m/s. Then the 10 m wind was recalculated with the agreed UTCI logarithmic profile and a z0 of 0.01. For the future heat wave situation of an air temperature of 40 °C, an MRT shade of 50 °C, an average water vapour pressure of 13.5 hPa, this change in wind speed results in a UTCI change of 0.3 K during the period of maximum MRT. For water vapour pressure of 20 hPa the change is only 0.1 K UTCI.

A recent comparison has been done by Zare et al., 2018, which shows that UTCI and PET are highly correlated. Urban and Kysely (2014) found for two regions in Bohemia that the simplification and underestimation of urban roughness only affects the prediction during cold spells, while PET and UTCI are both suitable to predict thermal discomfort during heat waves.

The maximum UTCI changes during extreme heat waves projected for the climate period 2050 from strong (32–38 °C UTCI) to very strong (38–46 °C UTCI) heat stress. This goes with other studies regarding future human thermal comfort. For example, Muthers et al. (2010) projected that even heat-related mortality could increase up to 129 % in Vienna until the end of the century, if no adaptation takes place. Matzarakis and Endler (2010) showed for Freiburg an increase of days with heat stress (PET>35 °C) in the order of 5 % (from 9.2 % for 1961–1990) per year.

4.2 City scale urban scenarios

4.2.1 Urban sprawl scenario

Urban sprawl of the Viennese agglomeration affects urban energy fluxes and temperature mainly in areas where new urban fabric is constructed on formerly vegetated areas. The sensible heat flux increases by up to +400 W/m^2 (not shown in the Figures), T_{min} by 1 K and the daily minimum UTCI by 1.3 K. No significant differences are simulated in the central districts, and no significant influence on the nocturnal UHI was found.

Kohler et al. (2017) presented a similar study for the Strasbourg–Kehl urban region (France–Germany). They conclude that under realistic assumptions urban sprawl until the year 2030 will not affect the UHI intensity significantly. Significant warming was only observed at atmospheric grid cells for which the urban fraction was increased more than 20 % compared to the initial case.

4.2.2 Optimized urban scenario

The optimized urban development scenario (OPT), which includes densification, slightly reduces air temperatures during the day, but clearly reduces them at night by 0.9 K. This leads to a slight reduction of nocturnal UHI by about 0.5 K. Also, the daily minimum UTCI is reduced by up to 0.7 K. The changed material properties can therefore counteract the negative effects of densification, which shows that the existing densification strategy of the city of Vienna (MA 18 (2014a+b) is promising. Salamanca et al. (2012) simulated a reduction of 1–2 K in UHI by assuming high albedo roofs and increased insulation for Madrid using WRF. Also, in their study the reduction of the heat ejected by air conditioning systems is mentioned as an important factor.

4.3 Local resilience measures

No coupled WRF-TEB simulations have been made for the quantification of the effect of single resilience measures. For this reason, the meteorological parameters above the urban canopy layer from the REF simulation has been used as forcing for offline simulations with SURFEX. With this modelling approach, the potential modification of the meteorological parameters above the urban canopy layer is not considered, and only the local effects can be seen, as if the rest of the city would still be built as REF. This part of the analysis shows what effects are to be expected locally if certain measures are not realized on a city scale but only on a local scale.

4.3.1 Albedo increase (ALB)

Increase of albedo is widely discussed as a cheap and effective measure to mitigate urban heat during summer heat episodes. e.g., Rafael et al. (2016) simulated using the WRF-SUEWS modelling system and roofs with an albedo of 80 % for Porto (Portugal) a maximum reduction in sensible heat flux of 62.8 W/m^2. Ramamurthy et al. (2015) showed that the wintertime penalty of white roofs, also for cool climates with 5 times more heating degree days than cooling degree days is insignificant compared to the summertime benefits. Žuvela-Aloise et al. (2018) simulated using MUKLIMO for Vienna a reduction of up to 6 summer

days when assuming a roof albedo of 70 %. In many cities this measure is widely discussed, e.g., Los Angeles (https://albedomap.lbl.gov/) or even has already been implemented (https://www.coolrooftoolkit.org/knowledgebase/white-roofs-in-brooklyn-new-york/). In Vienna itself there are no real life examples so far and potential legal difficulties and hindrances to implement bright roofs are yet unknown.

For street canyons, Weihs et al. (2018) found that wall albedo increases from 0.1 to 0.2 during periods of high solar irradiation in a canyon of height/width ratio 1 can reduce air temperature in the canyon by about 1 K, dependent on the canyon geometry and reduce UTCI by about the same value. Schrijvers et al. (2016) found a reduction in canyon air temperatures as well, and an increase of UTCI for high albedo values. For a height/width ratio of 0.5 Schrijvers et al. (2016) recommend a uniform albedo of 0.2, while for height/width ratio 1 they recommend a gradient from high albedo close to the roof to low albedo on the ground. Lee and Mayer (2018) found that during heat wave conditions also starting for low albedo values there is a positive linear relationship between albedo increases (0.2–0.8) within the canyon and the human thermal comfort index PET. Also, in this study the ALB scenario shows an increase in the UTCI human thermal comfort index. Therefore, only increases in roof albedo, not within the canyon are recommended.

4.3.2 Decreased thermal conductivity of urban materials (INS)

Increasing the albedo of a very low insulation roof from 0.05 to 0.75 is roughly equivalent to adding 14 cm of insulation thickness (Ramamurthy et al., 2015). While it is a challenge to maintain the reflective properties of a white roof, insulations have longer lasting effects (Ramamurthy et al., 2015). Roman et al. (2016) found that increasing insulation results in an increase in sensible heat flux and surface temperatures during the day and a reduction at night. Here the same patterns are found. Increases of daily maximum as well as decreases of minimum air temperature and UTCI of about 1 °C/1 K caused by insulation was found by Weihs et al. (2018) for historical climate. In this study, the daily maximum UTCI increases by more than 1.2 °C for a future heat wave with a 15 year return period. This is a clear negative effect of such a measure during daytime. However, the analysis of the energy fluxes during the heat wave shows that the longer the heat wave persists, the more the positive effects of building insulation prevail. Decreased thermal conductivity due to better building insulation is currently being adopted in widespread fashion in Vienna mainly to reduce the need for heating and reduce green house gas emissions during winter.

4.3.3 Increased building density (DEN)

Increase in building density within feasible ranges in Vienna has only limited effect on the sensible heat flux (an increase of 10 W/m^2 is simulated) and leads to a slight increase of the daily minimum UTCI (0.2 K) and maximum UTCI (up to 0.1 K). In the present study increasing height of buildings is not considered, as those are still restricted and there is still enough attic space to be developed and changes in building height are still low. Beyond 2050 it is possible that the building height will further increase and lead to a densification and could cause a damping of the diurnal air temperature and increased nocturnal temperatures (Coutts et al., 2007) caused by the reduced sky view. Without improving insulation this is likely to lead to an increase in mean air temperature and intensified UHI (Rad et al., 2017).

4.3.4 Evaporation of vegetation surfaces (GRR)

De Munck et al. (2018) found that green roofs have nearly no influence on street level air temperature, but are a good strategy to reduce energy consumption all year round. The evaporative cooling is strongly dependent on available soil moisture. Also, in this study the changes caused in the air canyon are marginal. The roof temperatures on the other hand are reduced by over 10 K. Also, here it could be seen, that the cooling potential of green roofs decline towards the end of the heat wave as latent heat flux goes down (Fig. 7d).

The maximum cooling generated during heat wave conditions caused by evapotranspiration of vegetation (not shading) within the city modelled by De Munck et al. (2018) varied between 0.5 and 2 K. The influence in terms of additional humidity caused by urban vegetation appears tolerable in comparison to the benefits. Additional water vapour pressure caused by forest vegetation compared to an open site in Oxford (UK) was quantified by Morecroft et al. (1998) to be below 2 hPa. As an extreme scenario Mahmood et al. (2008) could show that the influence of irrigation of agricultural fields during a long term measurement series increases the average near ground dew point temperature during growing season by 1.56 K in the North American Great Plains. Apart from this, the water vapour pressure of cities can also exceed the rural values due to different reasons (Kuttler et al., 2007). Maximum differences of 5 hPa between urban and rural (agricultural) areas were found by Fortuniak et al. (2006) for Łodz (Poland).

4.3.5 Photovoltaic panels on roofs (PVR)

The use of photovoltaic panels on roofs shows a slight reduction of temperature and thermal stress, which is in correspondence with findings from Masson et al. (2014), who found that solar panels can reduce the UHI by 0.2 K during day and 0.3 K at night. Weihs et al. (2018) found that photovoltaic used on roofs could lead to a temperature reduction of 1.5 K and a reduction of UTCI of 1.5 K. Therefore, this article encourages the use of photovoltaic on roofs within the city.

4.3.6 Shade and urban trees

(Tree) shade is a fundamental method to reduce mean radiant temperature (MRT) and thus improve human thermal comfort during clear sky conditions. Although we do not take into account the influence of tree shade on wall, road and canyon temperatures, we demonstrate the main influence of tree shade, which is the reduced direct radiation, by presenting the MRT in the sun and shade. So, the shade caused by buildings in this study can serve as a proxy for the influence of tree shade. By now tree shade has been implemented in one fork of TEB by Redon et al. (2017), but the code is not implemented in the main code tree yet. Wang et al. (2018) simulated the effect of radiative cooling (not evapotranspiration) of trees in the built environment of contiguous United States and found an average decrease in near surface air temperatures of 3.06 K. They show that not only do trees reduce incoming solar radiation during daytime they also increase radiative cooling at night. The ground heat flux is reduced in intensity in the shaded areas. Although the sensible heat flux is increased at night, it is strongly reduced during daytime. Matzarakis and Endler (2010) could show that by reducing global radiation by assuming tree shade in urban areas the number of days with heat stress could be reduced by more than 10 % in Freiburg. Ketterer and Matzarakis (2015) increased the number of trees in an area in Stuttgart and found a decrease in PET by 0.5 K at 22:00 CET but by maximum 27 K at 14:00 CET. Also, in this study we found a decrease of 26 K between the maximum MRT in the sun and in the shade.

The vitality of urban trees declined drastically over the last 3–4 decades (Bradshaw et al., 1995) and trees in Viennese parks (Drlik, 2010) and some species used in Viennese streets (Schimann, 2015; Neuwirth, 2015) and cities close to Vienna (Zeiler, 2015) are documented to be under stress due to multiple stressors including summer heat waves and there is likely to be a low shade transition phase between our historical tree stock dying and new more tolerant trees being planted and growing to a state where they can provide perceptible shade.

Generally urban green infrastructure improves air quality (Abhijith et al., 2017). Only in urban canyons air pollution can deteriorate (Abhijith et al., 2017), which can be avoided by reducing emissions.

5 Conclusions and Outlook

- We coupled WRF and TEB to simulate two urban development scenarios of Vienna, which are presented here, for two heat waves representative for present and future climatic conditions of the mid-21st century. Further extreme changes in building material parameters have been done to estimate the potential to reduce air temperatures and maintain human thermal comfort by altering buildings themselves.
- Global and regional climate change subject to the RCP8.5 scenario causes an increase in the mean daily maximum air temperature in Vienna by 7 K. The mean daily minimum air temperature will increase by 2–4 K. This increase is stronger than the global average. One important factor may be low soil water content in the agricultural region Northeast to Southeast of Vienna. This increase needs to be mitigated on a global level by reducing the emission of green house gases, but also land use on the regional level is of importance.
- City scale changes caused by urban growth or densification, which will mainly affect air temperature and human thermal comfort locally at the place where new urbanisation takes place and not to a significant degree in the central districts. Using a combination of adoption of nearly zero-energy building standard, as demanded by the European Union under the Energy Performance of Buildings Directive and increasing albedo of building materials on city scale, a maximum reduction of urban canyon temperature achieved by changes in urban parameters of 0.9 K for the minima and 0.2 K for the maxima is accomplished. The effects on human thermal comfort are even smaller with 0.7 K UTCI and 0.1 K UTCI respectively.
- Local scale changes of different adaptation measures show, that insulation of buildings used alone increases the maximum wall surface temperatures by more than 10 K or the maximum MRT in the canyon by 5 K.
- Therefore, measures to reduce MRT within the urban canyon preferably by tree shade, which was not possible to include in this study, are expected to complement the proposed measures and are urgently recommended.

This study concludes that the rising air temperatures expected by climate change puts an unprecedented heat burden on the Viennese inhabitants, which cannot easily be reduced by measures concerning buildings within the city itself. Therefore, in addition to those measures, small scale measures such as planting trees to provide shade, water sensitive planning in the agricultural plains surrounding Vienna and global measures such as the reduction of greenhouse gas emissions in order to reduce temperature extremes are required.

Acknowledgements

This research was mainly done within the project URBANIA (ACRP 8th call: KR14AC7K11944) funded by the Klima und Energiefond (KliEN). The finalization of the manuscript was done during a stay at NILU, Norway funded by the Marietta Blau scholarship of OeAD. We would like to thank Jürgen Preiss, the MA 18 and Beatrix Gasienica-Wawrytko for their feedback and comments. Finally, we want to thank the two reviewers who helped to improve the manuscript.

References

Abhijith, K.V., P. Kumar, J. Gallagher, A. McNabola, R. Baldauf, F. Pilla, B. Broderick, S. Di Sabatino, B. Pulvirenti, 2017: Air Pollution Abatement Performances of Green Infrastructure in Open Road and Built-up Street Canyon Environments – A Review. – Atmos. Env. **162**, 71–86 DOI:10.1016/j.atmosenv.2017.05.014.

Amtmann, M., N. Altmann-Mavaddat, 2014: Eine Typology österreichischer Wohngebäude. (in German) – Österreichische Energieagentur. – Austrian Energy Agency, TABULA/EPISCOPE, http://episcope.eu/fileadmin/tabula/public/docs/brochure/AT_TABULA_TypologyBrochure_AEA.pdf (last access: 05.08.2019).

APCC, 2014: Österreichischer Sachstandsbericht Klimawandel 2014 (AAR14). – Kromp-Kolb, H., N. Nakicenovic, K. Steininger, A. Gobiet, H. Formayer, A. Köppl, F. Prettenthaler, J. Stötter, J. Schneider, Verlag der Österreichischen Akademie der Wissenschaften, Wien, Österreich, 1096 pp.

Arnold, D., I. Schicker, P. Seibert, 2011: Towards high-resolution environmental modelling in the Alpine region. – In: Air Pollution Modeling and its Application XXI. 269–273, Springer.

Auer, I., U. Foelsche, R. Böhm, B. Chimani, L. Haimberger, H. Kerschner, K.A. Koinig, K. Nicolussi, C. Spötl, 2014: Vergangene Klimaänderung in Österreich, In: Österreichischer Sachstandsbericht Klimawandel 2014 (AAR14). – Austrian Panel on Climate Change (APCC), Verlag der Österreichischen Akademie der Wissenschaften, Wien, Österreich, 227–300.

Bador, M., L. Terray, J. Boé, S. Somot, A. Alias, A-L. Gibelin, B. Dubuisson, 2017: Future Summer Mega-Heatwave and Record-Breaking Temperatures in a Warmer France Climate. – Env. Res. Lett. **12**, 074025, 12, DOI: 10.1088/1748-9326/aa751c.

Bardow, A., D. Green, 2018: Low-Carbon Process Industries Through Energy Efficiency and Carbon Dioxide Utilisation, European Commission – Directorate-General for Research and Innovation, https://publications.europa.eu/en/publication-detail/-/publication/df9afa95-025d-11e8-b8f5-01aa75ed71a1/language-en (last access: 05.06.2019).

Berger, T., H. Formayer, R. Smutny, C. Neururer, R. Passawa, 2012: Auswirkungen des Klimawandelsauf den thermischen Komfort in Bürogebäuden (in German). – Berichte aus Energie- und Umweltforschung 7/2012, Bundesministerium für Verkehr, Innovation und Technologie, https://www.nachhaltigwirtschaften.at/resources/hdz_pdf/endbericht_1207_thermischer_komfort.pdf (last access 05.09.2012).

Boone, A., P. Samuelsson, S. Gollvik, A. Napoly L. Jarlan, E. Brun, B. Decharme, 2017: The interactions between atmosphere land surface model with a multi-energy balance (ISBA-MEB) option in SURFEXv8 Part 1: Model description. – Geosci. Model Develop. **10**, 843–872 DOI:10.5194/gmd-10-843-2017.

Bornstein, R., Q. Lin, 2000: Urban heat islands and summertime convective thunderstorms in Atlanta: Three case studies. – Atmos. Env. **34**, 507–516.

Bradshaw, A., B. Hunt, T. Walmsley, 1995: Trees in the Urban Landscape: Principles and Practice. – NY:E&FNSpon, London, NewYork,.

Bröde, P., D. Fiala, K. Blazejcyk, I. Holmér, G. Jendritzky, B. Kampmann, B. Tinz, G. Havenith, 2012: Deriving the operational procedure for the universal thermal climate index (utci). – Int. J. Biometeorol. **56**, 481–494.

Bueno, B., G. Pigeon, L.K. Norford, K. Zibouche, C. Marachadier, 2012: Development and evaluation of a building energy model integrated in the TEB scheme. – Geosci. Model Develop. **5**, 433–448 DOI:10.5194/gmd-5-433-2012.

Bundesministerium für Nachhaltigkeit und Tourismus (BMNT), 2016: Endbericht ÖKS15 – Klimaszenarien für Österreich, Daten – Methoden – Klimaanalyse. – Zentralanstalt für Meteorologie und Geodynamik (ZAMG), Wegener Center für Klima und globalen Wandel (WEGC) und dem Interfakultären Fachbereich Geoinformatik der Universität Salzburg (Z_GIS), https://www.bmnt.gv.at/umwelt/klimaschutz/klimapolitik_national/anpassungsstrategie/klimaszenarien.html (last access: 20.05.2019).

Cattiaux, J., H. Douville, R. Schoetter, S. Parey, P. Yiou, 2015: Projected increase in diurnal and interdiurnal variations of European summer temperatures. – Geophys. Res. Lett. **42**, 899–907 DOI:10.1002/2014GL062531.

Cordeau, E. , 2016: Les îlots morphologiques urbains (IMU) (in French). – IAU îdF, https://www.iau-idf.fr/fileadmin/NewEtudes/Etude_1270/Les_ilots_morphologiques_urbains.pdf (last access: 05.08.2019).

Coutts, A.M., J. Beringer, N.J. Tapper, 2007: Impact of Increasing Urban Density on Local Climate: Spatial and Temporal Variations in the Surface Energy Balance in Melbourne, Australia. – J. Appl. Meteor. Climatol. **46**, 477–493 DOI: 10.1175/JAM2462.1.

de Munck, C.S., A. Lemonsu, R. Bouzouidja, V. Masson, R. Claverie, 2013: The GREENROOF module (v7.3) for modelling green roof hydrological and energetic performances within TEB. – Geosci. Model Develop. **6**, 1941–1960. DOI: 10.5194/gmd-6-1941-2013.

de Munck, C.S., A. Lemonsu, V. Masson, J. Le Bras, M. Bonhomme, 2018: Evaluating the impacts of greening scenarios on thermal comfort and energy and water consumptions for adapting Paris city to climate change. – Urban Climate **23**, 260–286. DOI:10.1016/j.uclim.2017.01.003.

de Pee, A., D. Pinner, O. Roelofsen, K. Somers, E. Speelman, M. Witteveen, 2018: Decarbonization of industrial sectors: the next frontier. – McKinsey & Company, https://www.mckinsey.com/business-functions/sustainability/our-insights/how-industry-can-move-toward-a-low-carbon-future (last access: 05.06.2019).

Donner, L.J., B.L. Wyman, R.S. Hemler, L.W. Horowitz, Y. Ming, M. Zhao, J.-C. Golaz, P. Ginoux, S.J. Lin, M.D. Schwarzkopf, J. Austin, G. Alaka, W.F. Cooke, T.L. Delworth, S.M. Freidenreich, C.T. Gordon, S.M. Griffies, I.M. Held, W.J. Hurlin, S.A. Klein, T.R. Knutson, A.R. Langenhorst, H.-C. Lee, Y. Lin, B.I. Magi, S.L. Malyshev, P.C.D. Milly, V. Naik, M.J. Nath, R. Pincus, J.J. Ploshay, V. Ramaswamy, C.J. Seman, E. Shevliakova, J.J. Sirutis, W.F. Stern, R.J. Stouffer, R.J. Wilson, M. Winton, A.T. Wittenberg, F. Zeng, 2011: The Dynamical Core, Physical Parameterizations, and Basic Simulation Characteristics of the Atmospheric Component AM3 of the GFDL Global Coupled Model CM3. – Journal of Climate **24**, 13, 3484–3519.

Dou, Y. , 2014: The influence of urban planning on urban thermal comfort. – Master Thesis, Wageningen University, the Netherlands, https://www.wur.nl/upload_mm/8/f/f/a3db8019-a442-4270-9a43-d7e06e834169_Dou_Yuehan_THE_LUP80436_201407.pdf (last access: 2019.08.29).

Duchez, A., E. Frajka-Williams, S.A. Josey, D.G. Evans, J.P. Grist, R. Marsh, G.D. McCarthy, B. Sinha, D.I. Berry, J.J.M. Hirschi, 2016: Drivers of Exceptionally Cold North Atlantic Ocean Temperatures and Their Link to the

2015 European Heat Wave. – Environmental Research Letters, **11**, 7, 074004.

Drlik, S., 2010: Klimawandelanpassung der Pflege und Erhaltung öffentlicher Grünanlagen in Grossstädten unter Berücksichtigung des Konzepts der Nachhaltigen Entwicklung, untersucht am Fallbeispiel Wien. (in German) – Dissertation, https://zidapps.boku.ac.at/abstracts/download.php?dataset_id=7703&property_id=107 (last access: 11.10.2019).

EEA (European Environment Agency), 2012: Corine land cover data set 2012, https://www.eea.europe.eu/data-and-maps/data/clc-2012-raster (last access: 23.05.2018).

Erell, E., D. Pearlmutter, T. Williamson, 2011: Urban Microclimate – Designing the Spaces Between Buildings. – Earthscan, Washington, USA, 266 pp.

Fallmann, J., R. Forkel, S. Emeis, 2016: Secondary effects of urban heat island mitigation measures on air quality. – Atmos. Env. **125**, 199–211, DOI:10.1016/j.atmosenv.2015.10.094.

Fanger, P.O. , 1970: Thermal Comfort, Analysis and Applications in Environmental Engineering. – McGraw-Hill Company, US, 244 pp.

Fiala, D., K.J. Loma, M. Stohrer, 2001: Computer prediction of human thermoregulatory and temperature responses to a wide range of environmental conditions. – Int. J. Biometeorol. **45**, 143–159.

Fischer, E.M., S.I. Seneviratne, 2007: Soil Moisture – Atmosphere Interactions during the 2003 European Summer Heat Wave. – J. Clim., 20, 5081–5099, DOI:10.1175/JCLI4288.1.

Fisher, R., L. Tippett, 1928: Limiting forms of the frequency distributions of the largest or smallest member of a sample. – Proc Camb Philos Soc. **24**, 180–190.

Formayer, H., P. Haas., M. Hofstätter., S. Radanovics, H. Kromp-Kolb, 2007: Räumlich und zeitlich hochaufgelöste Temperaturszenarien für Wien und ausgewählte Analysen bezüglich Adaptionsstrategien. – Bericht im Auftrag der Wiener Umweltschutzabteilung – MA 22 der Stadt Wien gemeinsam mit der MA 27 – EU-Strategie und Wirtschaftsentwicklung, https://www.wien.gv.at/wirtschaft/standort/pdf/temperaturszenarien.pdf (last access: 05.08.2019).

Fortuniak, K., K. Klysik, J. Wibig, 2006: Urban–Rural Contrasts of Meteorological Parameters in Lódz. – Theor. Appl. Climatol. **84**, 91–101, DOI:10.1007/s00704-005-0147-y.

Gabriel, K.M.A., W.R. Endlicher, 2011: Urban and rural mortality rates during heat waves in Berlin and Brandenburg, Germany. – Env. Poll. **159**, 2044–2050.

Gobiet, A., S. Kotlarski, M. Beniston, G. Heinrich, J. Rajczak, M. Stoffel, 2014: 21st century climate change in the European Alps – A review. – Sci. Total Env. **493**, 1138–1151 DOI:10.1016/j.scitotenv.2013.07.050.

Grimmond, C.S. B, M. Roth, T.R. Oke, Y.C. Au, M. Best, R. Betts, G. Carmichael, H. Cleugh, W. Dabberdt, R. Emmanuel, E. Freitas, K. Fortuniak, S. Hanna, P. Klein, L.S. Kalkstein, C.H. Liu, A. Nickson, D. Pearlmutter, D. Sailor, J. Voogt, 2010: Climate and More Sustainable Cities: Climate Information for Improved Planning and Management of Cities (Producers/Capabilities Perspective). – Proc. Env. Sci. **1**, 247–274.

Hartmann, D.L. , 1994: Global Physical Climatology. - Academic Press, 411 pp.

Hutter, H. P, H. Moshammer, P. Wallner, B. Leitner, M. Kundi, 2007: Heatwaves in Vienna: effects on mortality. – Wien Klin. Wochenschr. **119**, 223–227.

IPCC, 2013: The Physical Science Basis, Contribution of Working Group I to the Fifth Assessment Report of the Intergovernmental Panel on Climate Change. – In: Climate Change 2013, Stocker, T.F., D. Qin, G-K. Plattner, M.M.B. Tignor, S.K. Allen, J. Boschung, A. Nauels, Y. Xia, V. Bex, P.M. Midgley, Cambridge University Press, Cambridge, United Kingdom and New York, NY, USA, 1535 pp.

Jacob, D., J. Petersen, B. Eggert, A. Alias, O.B. Christensen, L.M. Bouwer, A. Braun, A. Colette, M. Déqué, G. Georgievski, E. Georgopoulou, A. Gobiet, L. Menut, G. Nikulin, A. Haensler, N. Hempelmann, C. Jones, K. Keuler, S. Kovats, N. Kröner, S. Kotlarski, A. Kriegsmann, E. Martin, E. v. Meijgaard, C. Moseley, S. Pfeifer, S. Preuschmann, C. Radermacher, K. Radtke, D. Rechid, M. Rounsevell, P. Samuelsson, S. Somot, J. -F. Soussana, C. Teichmann, R. Valentini, R. Vautard, B. Weber, P. Yiou, 2014: EURO-CORDEX: new high-resolution climate change projections for European impact research. – Reg. Env. Change. **14**, 2, 563–578 DOI:10.1007/s10113-013-0499-2.

Jasper, K., P. Calanca, J. Fuhrer, 2006: Changes in summertime soil water patterns in complex terrain due to climatic change. – J. Hydrol. **327**, 3–4, 550–563 DOI:10.1016/j.jhydrol.2005.11.061.

Jendritzky, G., R. De Dear, G. Havenith, 2012: UTCI – Why another thermal index? – Int. J. Biometeorol. **56**, 421–428.

Jones, R., J. Murphy, D. Hassell, R. Taylor, 2001: Ensemble mean changes in a simulation of the European climate of 2071–2100 using the new Hadley Centre regional modelling system HadAM3H/HadRM3H. – Hadley Centre, Met Office, Bracknell, UK. http://prudence.dmi.dk/public/publications/hadley_200208.pdf (last access: 06.06.2019).

Kalisa, E., S. Fadlallah, M. Amani, L. Nahayo, G. Habiyaremye, 2018: Temperature and air pollution relationship during heatwaves in Birmingham, UK. – Sustain. Cities Soc. **43**, 111–120.

Kennedy, C., J. Steinberger, B. Gasson, Y. Hansen, T. Hillman, M. Havránek, D. Pataki, A. Phdungsilp, A. Ramaswami, G.V. Mendez, 2009: Greenhouse Gas Emissions from Global Cities. – Environmental Science & Technology **43**, 7297–7302. DOI:10.1021/es900213p.

Ketterer, C., A. Matzarakis, 2015: Comparison of Different Methods for the Assessment of the Urban Heat Island in Stuttgart, Germany. – Int. J. Biometeorol. **59**, 1299–1309 DOI:10.1007/s00484-014-0940-3.

Ketterer, C., M. Gangwisch, D. Fröhlich, A. Matzarakis, 2017: Comparison of Selected Approaches for Urban Roughness Determination Based on Voronoi Cells. – Int. J. Biometeorol. **61**, 1, 189–98. DOI:10.1007/s00484-016-1203-2.

Kim, J., J. Kyselý, 2009: Mortality during heat waves in South Korea, 1991 to 2005: How exceptional was the 1994 heat wave? – Climate Res. **38**, 105–116. DOI:10.3354/cr00775.

Kohler, M., C. Tannier, N. Blond, R. Aguejdad, A. Clappier, 2017: Impacts of several urban-sprawl countermeasures on building (space heating) energy demands and urban heat island intensities. A case study. – Urban Climate **19**, 92–121. DOI:10.1016/j.uclim.2016.12.006.

Kornhuber, K., V. Petoukhov, S. Petri, S. Rahmstorf, D. Coumou, 2017: Evidence for wave resonance as a key mechanism for generating high-amplitude quasi-stationary waves in boreal summer. – Climate Dynamics, **49**, 5–6, 1961–1979 DOI:10.1007/s00382-016-3399-6.

Krispel, S., M. Peyerl, P. Weihs, G. Maier, 2017: Reduction of Urban Heat Islands with Whitetopping. –Bauphysik. **39**, 1, 33–39.

Kuttler, W., S. Weber, J. Schonnefeld, A. Hesselschwerdt, 2007: Urban/rural atmospheric water vapour pressure differences and urban moisture excess in Krefeld, Germany. – International Journal of Climatology, **27**, 14, 2005–2015. DOI:10.1002/joc.1558.

Kyselý, J., J. Kalvová, V. Kveton, 2000: Heat waves in the South Moravian region during the period 1961–1995. – Studia Geophys Geodaet. **44**, 57–72.

Landsberg, H.E., 1981: The Urban Climate. – Academic Press, 275 pp.

Lee, H., H. Mayer, 2018: Thermal comfort of pedestrians in an urban street canyon is affected by increasing albedo of building walls. – Int. J. Biometeorol. **62**, 1199–1209. DOI: 10.1007/s00484-018-1523-5.

Lemonsu, A., C.S.B. Grimmond, V. Masson, 2004: Modeling the surface energy balance of the core of an old Mediterranean City: Marseille. – J. Appl. Meteor. Climatol. **43**, 312–327.

Lemonsu, A., V. Masson, L. Shashua-Bar, E. Erell, D. Pearlmutter, 2012: Inclusion of vegetation in the Town Energy Balance model for modelling urban green areas. – Geosci. Model Develop. **5**, 1377–1393.

Lemonsu, A., R. Kounkou-Arnaud, J. Desplat, J.L. Salagnac, V. Masson, 2013: Evolution of the Parisian urban climate under a global changing climate. – Climatic Change **116**, 679–692.

Leuprecht, A., B. Chimani, M. Hofstätter, M. Kerschbaumer, S. Kienberger, M. Kottek, H. Truhetz, A. Lexer, S. Pessenteiner, 2017: ÖKS15 bias corrected Euro-Cordex models, version 2. – https://data.ccca.ac.at/group/oks15 (last access: 05.09.2019).

Li, Y., R. Babcock, 2014: Green roofs against pollution and climate change. A review. – Agro. Sustain. Develop. **34**, 695–705. DOI:10.1007/s13593-014-0230-9.

MA (Magistratsabteilung) 18 – Stadtentwicklung und Stadtplanung, 2005: Urban Development Plan Vienna 2005 – STEP05, https://www.wien.gv.at/stadtentwicklung/strategien/step/step05/download/pdf/step-gesamt.pdf (in German), https://w.at/stadtentwicklung/strategien/step/step05/download/pdf/step05kurz-en.pdf (last access: 05.08.2019).

MA (Magistratsabteilung) 18 – Stadtentwicklung und Stadtplanung, 2011: Patterns for new urban developments. – Werkstattberichte der Stadtentwicklung Wien Nr. **116**, https://www.wien.gv.at/stadtentwicklung/studien/b008197.html (last access: 05.08.2019).

MA (Magistratsabteilung) 18 – Stadtentwicklung und Stadtplanung, 2014a: Smart City Wien – Framework Strategy, https://www.wien.gv.at/stadtentwicklung/studien/pdf/b008384b.pdf (last access: 05.08.2019).

MA (Magistratsabteilung) 18 – Stadtentwicklung und Stadtplanung, 2014b: Urban Development Plan Vienna 2015 – STEP 2025 (in German), www.step.wien.at (last access: 05.08.2019).

MA (Magistratsabteilung) 22 – Umweltschutz, 2018: Urban Heat Island Strategy, Vienna. – https://www.wien.gv.at/umweltschutz/raum/pdf/uhi-strategieplan-englisch.pdf (last access: 2019.04.12).

Mahmood, R., K.G. Hubbard, R.D. Leeper, S.A. Foster, 2008: Increase in Near-Surface Atmospheric Moisture Content due to Land Use Changes: Evidence from the Observed Dewpoint Temperature Data. – Mon. Wea. Rev. **136**, 1554–1561 DOI:10.1175/2007MWR2040.1.

Masson, V. , 2000: A physically-based scheme for the urban energy budget in atmospheric models. – Bound-Layer Meteor. **94**, 357–397 DOI:10.1023/A:1002463829265.

Masson, V., C.S.B. Grimmond, T.R. Oke, 2002: Evaluation of the Town Energy Balance (TEB) scheme with direct measurements from dry districts in two cities. – J. Appl. Meteor. **41**, 1011–1026.

Masson, V., M. Bonhomme, J.-L. Salagnac, X. Briottet, A. Lemonsu, 2014: Solar panels reduce both global warming and urban heat island. – Front. Environ. Sci. **2**, published online. DOI:10.3389/fenvs.2014.00014.

Matzarakis, A., C. Endler, 2010: Climate change and thermal bioclimate in cities: Impacts and options for adaptation in Freiburg, Germany. – Int. J. Biometeorol. **54**, 479–83. DOI: 10.1007/s00484-009-0296-2.

Matzarakis, A., S. Muthers, E. Koch, 2011: Human biometeorological evaluation of heat-related mortality in Vienna. – Theor. Appl. Climatol. **105**, 1–10. DOI:10.1007/s00704-010-0372-x.

McMichael, A.J., R. Woodruff, K. Whetton, N. Hennessy, N. Nicholls N., S. Hales, A. Woodward, T. Kjellstrom, 2003: Human Health and Climate Change in Oceania: Risk Assessment Canberra. – Commonwealth Department of Health and Ageing, http://citeseerx.ist.psu.edu/viewdoc/download?doi=10.1.1.183.6422&rep=rep1&type=pdf (last access: 05.08.2019).

Mayer, H., P. Höppe, 1987: Thermal comfort of man in different urban environments. – Theor. Appl. Climatol. **38**, 43–49 DOI: 10.1007/BF00866252.

Michalakes, J., S. Chen, J. Dudhia, L. Hart, J. Klemp, J. Middlecoff, W. Skamarock, 2001: Development of a next-generation regional weather research and forecast model. – In: World Scientific (Pub.): Developments in Teracomputing. 269–276.

Michelozzi, P., F. De Donato, G. Accetta, F. Forastiere, M. D'Ovidio, C.A. Perucci, 2004: Impact of heatwaves on mortality – Rome, Italy – June–August 2003. – JAMA. **291**, 2537–2538. DOI:10.1001/jama.291.21.2537.

Morecroft, M.D., M.E. Taylor, H.R. Oliver, 1998: Air and Soil Microclimates of Deciduous Woodland Compared to an Open Site. – Agricult. Forest Meteor. **90**, 141–56. DOI: 10.1016/S0168-1923(97)00070-1.

Morini, E., A. Touchaei, B. Castellani, F. Rossi, F. Cotana, 2016: The Impact of Albedo Increase to Mitigate the Urban Heat Island in Terni (Italy) Using the WRF Model. – Sustainability **8**, 999. DOI:10.3390/su8100999.

Muthers, S., A. Matzarakis, E. Koch, 2010: Climate change and mortality in Vienna – a human biometeorological analysis based on regional climate modeling. – Int. J. Environ. Res. Public Health. **7**, 2965–2977. DOI:10.3390/ijerph7072965.

Neuwirth, C., 2015: Effects of climate on Urban Trees in Vienna. – Master Thesis (in German) at the Institute of Soil Bioengineering and Landscape Construction, University of Natural Resources and Life Sciences, Vienna, https://zidapps.boku.ac.at/abstracts/download.php?dataset_id=11754&property_id=107 (last access: 11.10.2019).

Offerle, B., P. Jonsson, I. Eliasson, C.S.B. Grimmond, 2005: Urban modification of the surface energy balance in the West African Sahel: Ouagadougou, Burkina Faso. – J. Climate **18**, 3983–3995.

Oke, T. R., 1982: The energetic basis of the urban heat island. – Quart. J. Roy. Meteor. Soc. **108**, 1–24. DOI:10.1002/qj.49710845502.

Oke, T. R., 1987: Boundary Layer Climates. – Routledge, Taylor&Francis Group, 464 pp.

ÖROK, 2017: ÖROK Atlas (in German), https://www.oerok-atlas.at/#indicator/65 (last access: 05.08.2019).

Otani, H., G. Takayuki, G. Heita, S. Minayuki, 2017: Time-of-day effects of exposure to solar radiation on thermoregulation during outdoor exercise in the heat. – Chronobiol. Int. **34**, 1224–1238.

Pearlmutter, D., P. Berliner, E. Shaviv, 2005: Evaluation of urban surface energy fluxes using an open-air scale model. – Bound.-Layer Meteor. **44**, 532–545.

Pigeon, G., K. Zibouche, B. Bueno, J. Le Bras, V. Masson, 2014: Improving the capabilities of the Town Energy Balance model with up-to-date building energy simulation algorithms:

an application to a set of representative buildings in Paris. – Energy Build. **76**, 1–14.

Pineda, N., O. Jorba, J. Jorge, J. Baldasano, 2004: Using NOAAAVHR Rand SPOT VGT data to estimate surface parameters: application to a mesoscale meteorological model. – Int. J. Remote Sens. **25**, 129–143.

PGO (Planungsgemeinschaft Ost), 2011: stadtregion+ (in German), Planungskooperation zur räumlichen Entwicklung der Stadtregion Wien Niederösterreich Burgenland, http://www.planungsgemeinschaft-ost.at/fileadmin/root_pgo/Studien/Raumordnung/Zwischenbericht_Stadtregion.pdf (last access: 05.08.2019).

Rad, H.R., M. Rafieian, H. Sozer, 2017: Evaluating the effects of increasing of building height on land surface temperature. – Int. J. Urban Manage Energy Sustain. **1**, 11–16. DOI:10.2034/ijumes.2017.01.01.002.

Rafael, S., H. Martins, E. Sá, D. Carvalho, C. Borrego, M. Lopes, 2016: Influence of urban resilience measures in the magnitude and behaviour of energy fluxes in the city of Porto (Portugal) under a climate change scenario. – Sci. Total Environ. **566–567**, 1500–1510, DOI: 10.1016/j.scitotenv.2016.06.037.

Ramamurthy, P., T. Sun, K. Rule, E. Bou-Zeid, 2015: The Joint Influence of Albedo and Insulation on Roof Performance: A Modeling Study. – Energy Build. **102**, 317–27. DOI: 10.1016/j.enbuild.2015.06.005.

Redon, E.C., A. Lemonsu, V. Masson, B. Morille, M. Musy, 2017: Implementation of street trees within the solar radiative exchange parameterization of TEB in SURFEX v8.0. – Geosci. Model Develop. **10**, 385–411. DOI: 10.5194/gmd-10-385-2017.

Roman, K.K., T. O'Brien, J.B. Alvey, O. Woo, 2016: Simulating the Effects of Cool Roof and PCM (Phase Change Materials) Based Roof to Mitigate UHI (Urban Heat Island) in Prominent US Cities. – Energ. **96**, 103–17, DOI:10.1016/j.energy.2015.11.082.

Salamanca, F., A. Martilli, C. Yagüe, 2012: A Numerical Study of the Urban Heat Island over Madrid during the DESIREX, 2008: Campaign with WRF and an Evaluation of Simple Mitigation Strategies. – Int. J. Climatol. **32**, 2372–2386. DOI:10.1002/joc.3398.

Schicker, I., D. Arnold Arias, P. Seibert, 2016: Influences of updated land-use datasets on WRF simulations for two Austrian regions. – Meteor. Atmos. Phys. **128**, 279–301 DOI: 10.1007/s00703-015-0416-y.

Schimann, J., 2015: The effect of climate on trees in streets of Vienna. – Bachelor Thesis (in German) at the Institute of Soil Bioengineering and Landscape Construction, University of Natural Resources and Life Sciences, Vienna.

Schnell, J.L., M.J. Prather, 2017: Co-occurrence of extremes in surface ozone, particulate matter, and temperature over eastern North America. – Proc. Natl. Acad. Sci. USA. **114**, 2854–2859 DOI:10.1073/pnas.1614453114.

Schreier, S., I. Suomi, P. Bröde, H. Formayer, H.E. Rieder, I. Nadeem, G. Jendritzky, E. Batchvarova, P. Weihs, 2013: The uncertainty of UTCI due to uncertainties in the determination of radiation fluxes derived from numerical weather prediction and regional climate model simulations. – Int. J. Biometeorol. **57**, 2, 207–223.

Schrijvers, P.J.C., H.J.J. Jonker, S.R. de Roode, S. Kenjereš, 2016: The Effect of Using a High-Albedo Material on the Universal Temperature Climate Index within a Street Canyon. – Urban Climate **17**, DOI:10.1016/j.uclim.2016.02.005.

Seneviratne, S.I., R. Wartenburger, B.P. Guillod, A.L. Hirsch, M.M. Vogel, V. Brovkin, D.P. van vuuren, N. Schaller, L. Boysen, K.V. Calvin, J. Doelman, P. Greve, P. Havlik, F. Humpenöder, T. Krisztin, D. Mitchell, A. Popp, K. Riahi, J. Rogelj, C.-F. Schleusser, J. Sillmann, E. Stehfest, 2018: Climate extremes, land–climate feedbacks and land-use forcing at 1.5 °C. – Philosophical Transactions of the Royal Society A: Mathematical, Physical and Engineering Sciences **376**, 2119, DOI:10.1098/rsta.2016.0450.

Sharifi, A., Y. Yamagata, 2018: Resilience-Oriented Urban Planning. – In: Yamagata, Y., A. Sharifi (Eds.): Resilience-Oriented Urban Planning. – Lecture Notes in Energy **65**, 3–27. DOI:10.1007/978-3-319-75798-8_1.

Skamarock, W.C., J.B. Klemp, J. Dudhia, D.O. Gill, D.M. Barker, M.G. Duda, X.-Y. Huang, W. Wang, J.G. Powers, 2008: A Description of the Advanced Research WRF Version 3. – NCAR. Tech. Note NCAR/TN-475+STR, 113 pp.

Steadman, R.G. , 1979a: The Assessment of Sultriness. Part I: A Temperature-Humidity Index Based on Human Physiology and Clothing Science. – J. Appl. Meteor. **18**, 861–873. DOI: 10.1175/1520-0450(1979)018<0861:TAOSPI>2.0.CO;2.

Steadman, R. G., 1979b: The Assessment of Sultriness. Part II: Effects of Wind, Extra Radiation and Barometric Pressure on Apparent Temperature. – J. Appl. Meteor. **18**, 874–885 DOI: 10.1175/1520-0450(1979)018<0874:TAOSPI>2.0.CO;2.

Stewart, I.D., T.R., Oke, 2012: Local climate zones for urban temperature studies. – Bull. Amer. Meteor. Soc. **93**, 1879–1900.

Stull, R. B., 1988: An Introduction to Boundary Layer Meteorology. – Kluwer academic Publishers, Dordrecht-Boston-London.

Switanek, M.B., P.A. Troch, C.L. Castro, A. Leuprecht, H.-I. Chang, R. Mukherjee, E.M.C. Demaria, 2017: Scaled distribution mapping: a bias correction method that preserves raw climate model projected changes. – Hydrol. Earth Syst. Sci. **21**, 2649–2666. DOI:10.5194/hess-21-2649-2017.

Taha, H., S. Douglas, J. Haney, 1997: Mesoscale meteorological and air quality impacts of increased urban albedo and vegetation. – Energy Build. **25**, 169–177. DOI:10.1016/S0378-7788(96)01006-7.

Tan, J., Y. Zheng, G. Song, L. Kalkstein, A. Kalkstein, X. Tang, 2007: Heatwave Impacts on Mortality in Shanghai: 1998 to 2003. – Int. J. Biometeorol. **51**, 193.

Taylor, K.E., R.J. Stouffer, G.A. Meehl, 2012: An Overview of CMIP5 and the Experiment Design. – Bull. Am. Meteorol. Soc. **93**, 4, 485–498 DOI:10.1175/BAMS-D-11-00094.1.

Urban, A., J. Kyselý, 2014: Comparison of UTCI with Other Thermal Indices in the Assessment of Heat and Cold Effects on Cardiovascular Mortality in the Czech Republic. – Int. J. Env. Res.Public Health **11**, 952–67. DOI:10.3390/ijerph110100952.

Ürge-Vorsatz, D., C. Rosenzweig, R.J. Dawson, R.S. Rodriguez, X. Bai, A.S. Barau, K.C. Seto, S. Dhakal, 2018: Locking in Positive Climate Responses in Cities. – Nature Climate Change **8**, 174–77. DOI:10.1038/s41558-018-0100-6.

Valleron, A.J., A. Boumendil, 2004: Epidemiology and heat waves: Analysis of the 2003 episode in France. – C.R. Biology **327**, 1125–41.

Vidale, P.L., D. Lüthi, R. Wegmann, C. Schär, 2007: European summer climate variability in a heterogeneous multimodel ensemble. – Climatic Change **81**, S1, 209–232. DOI: 10.1007/s10584-006-9218-z.

Vogel, M.-M., 2018: Temperature extremes in a changing climate – Processes, emergent constraints and impacts. – Doctoral Thesis at ETH Zürich, DOI:10.3929/ethz-b-000323120.

Wang, C., Z.-H. Wang, J. Yang. 2018: Cooling Effect of Urban Trees on the Built Environment of Contiguous United States. – Earth's Future **6**,1066–1081. DOI:10.1029/2018EF000891.

Weihs, P., H. Staiger, B. Tinz, E. Batchvarova, H. Rieder, L. Vuilleumier, M. Maturilli, G. Jendritzky, 2012: The uncertainty of UTCI due to uncertainties in the determination of radiation fluxes derived from measured and observed meteorological data. – Int. J. Biometeorol. **56**, 537–555.

Weihs, P., S. Zamini, S. Krispel, S. Oswald, M. Peyerl, M. Revesz, A. Schneider, H. Trimmel, 2018: Optimierung reflektierender Materialien und Photovoltaik im Stadtraum bezüglich Strahlungsbilanz und Bioklimatik (PVOPTI-Ray). (in German), Berichte aus Energie- und Umweltforschung 18/2018 Nachhaltig wirtschaften, Bundesministerium für Verkehr, Innovation und Technologie, Wien, https://nachhaltigwirtschaften.at/resources/sdz_pdf/schriftenreihe_2018-18_pvoptiray.pdf (last access: 05.08.2019).

Zampieri, M., F. D'Andrea, R. Vautard, P. Ciais, N. de Noblet-Ducoudré, P. Yiou, 2009: Hot European Summers and the Role of Soil Moisture in the Propagation of Mediterranean Drought. – J. Climate **22**, 4747–4758. DOI: 10.1175/2009JCLI2568.1.

Zare, S., N. Hasheminejad, H.E. Shirvan, R. Hemmatjo, K. Sarebanzadeh, S. Ahmadi, 2018: Comparing Universal Thermal Climate Index (UTCI) with selected thermal indices/environmental parameters during 12 months of the year. – Wea. Climate Extremes **19**, 49–57. DOI:10.1016/j.wace.2018.01.004.

Zeiler, S. , 2015: Auswirkungen des Klimas auf Stadtbäume im Bezirk Korneuburg/Niederösterreich. – Master Thesis (in German), Institute of Soil Bioengineering and Landscape Construction, University of Natural Resources and Life Sciences, Vienna, 231 pp, https://zidapps.boku.ac.at/abstracts/download.php?dataset_id=12169&property_id=107 (last access: 11.10.2019).

Zhang, H., Y. Wang, T. Park, Y. Deng, 2017: Quantifying the relationship between extreme air pollution events and extreme weather events. – Atmos. Res. **188**, 64–79.

Zommers, Z., K. Alverson, 2018: Resilience – The Science of Adaptation to Climate Change. – Elsevier, Amsterdam, Oxford, Camebridge, 354 pp.

Žuvela-Aloise, M., K. Andre, K., H. Schwaiger, D.N. Bird, H. Gallaun, 2018: Modelling reduction of urban heat load in Vienna by modifying surface properties of roofs. – Theor. Appl. Climatol. **131**, 1005–1018. DOI:10.1007/s00704-016-2024-2.

The pdf version (Adobe Java Script must be enabled) of this paper includes an electronic supplement:
Table of content – Electronic Supplementary Material (ESM)

Figure A-1